Experimental Electric Vehicle

Scientific papers presented at:

EVC symposium VI, Baltimore 1981
Drive Electric, Amsterdam 1982

Eindhoven University of Technology

EVC No. 8115

Theoretical Prediction of Electric Vehicle Energy Consumption and Battery State-of-Charge During Arbitrary Driving Cycles

L. A. M. van Dongen
Eindhoven University of Technology

R. van der Graaf
Eindhoven University of Technology

W. H. M. Visscher
Eindhoven University of Technology

EVC SYMPOSIUM VI
Baltimore Convention Center
Baltimore, Maryland
October 21-23, 1981

Electric Vehicle Council
1111 19th Street, N.W.
Washington, D.C. 20036
U.S.A.
(202) 828-7516

ABSTRACT

In order to obtain a reliable comparison of electric vehicle propulsion systems in an early state of development, a digital computer simulation program has been developed. Starting with the road-load the power flow through the entire drive line is calculated for a specified driving cycle, including regenerative braking. The energy-efficiency characteristics of motor and transmission are taken in account as a function of both torque and speed. Experimentally obtained component characteristics are used to define the drive line. In the program a battery state-of-charge model for the lead-acid battery is implied, which is based on the non-linear ampere-hour capacity versus normalized constant discharge curve. As the vehicle proceeds on the chosen driving cycle cumulative charge reduction is determined. Battery voltage is modeled as a function of battery current and depth of discharge. Results for different drive trains are discussed. It is shown that the energy use of a propulsion train with a variable transmission ratio is lower than that of a drive system with a fixed gear ratio. It appears that this simulation gives a good insight in the energy use and losses of the various parts of the drive train.

1. INTRODUCTION

Many motor-car manufacturers are developing and testing several power train systems in various electric vehicles. Due to different vehicle characteristics and testing conditions it is nearly impossible to obtain a reliable comparison of these drive trains. For this reason a multi-disciplinary working group at the Eindhoven University of Technology has set out to construct and test various drive systems in the same vehicle and under identical conditions.

In order to optimize the operating range and the consumption of primary energy, the components of the drive system have to be matched. Specifically this matching of components is important if regenerative braking is considered, since the braking power has to pass along the drive train twice.

It is difficult to dertermine the influence of different drive train systems on the vehicle energy use and the operating range because:

- the efficiencies of the component parts of a power train system are not constant, but can vary strongly for each operating point (torque and speed) of the relevant component.
- even during standard duty cycles the wheel-power requirements - and consequently the component efficiencies - are seldom reproducible.
- the total amount of energy which can be delivered by the battery depends on the present and past rates of discharge and/or charge.

Therefore a detailed vehicle simulation program has been developed in order to compare and match different drive trains. Within the program several mathematical models for battery, chopper, motor, gearbox, torque converter and vehicle can be stored in the form of both tables and equations. The technique of assembling a drive train and a vehicle from models, in which the measured and/or estimated efficiencies are computable for each operating point, makes the program extremely flexible and new models can be created and added at any time. The drive train model can be applied to simulate the energy use of an electric vehicle during a specified test cycle. Examples of interesting output variables are: battery voltage, current and state-of-charge, distance covered, average gearbox efficiency and average motor efficiency.

Computer simulation of the power train system with respect to energy economy offers the following benifits:

- reproducibility of results; no influences beyond control as weather conditions
- fast response time; evaluation of alternatives is possible in a short period of time
- evaluation of component changes is possible before and during vehicle development; consequent savings in expenditures.

In this paper the vehicle simulation model will be described for a given electric vehicle drive system.

2. VEHICLE MODEL

In order to obtain reliable simulation results an accurate analysis of the vehicle resistance is indispensable. The vehicle road-load is the sum of aerodynamic resistance, rolling resistance and grade resistance.

The air resistance of the vehicle can be expressed as

$$F_w = \tfrac{1}{2} \rho * V_{res}^2 * A_F * C_w \qquad (1)$$

where

F_w	aerodynamic resistance	(N)
ρ	specific air density	(kg/m^3)
V_{res}	relative vehicle speed with respect to the air	(m/s)
A_F	frontal surface area of the vehicle	(m^2)
C_w	aerodynamic drag coefficient	(-)

The drag coefficient is dependent on the shape of the vehicle only and varies between 0.30 for well streamlined motor-cars and 0.55 for ill streamlined passenger cars.

The rolling resistance of the vehicle is given by

$$F_r = f_r * F_N \qquad (2)$$

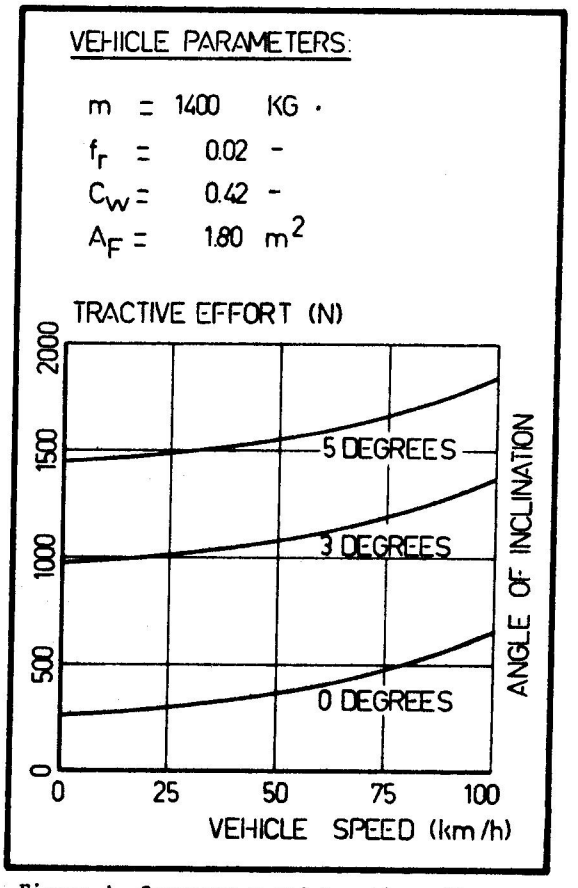

Figure 1. Constant speed tractive effort.

where

F_r	rolling resistance	(N)
f_r	rolling resistance factor of the wheels	(-)
F_N	load on the wheels perpendicular to the road surface	(N)

Concerning the rolling resistance factor the development of radial-ply tyres has paid dividends. In this work the use of tyres with a rolling resistance coefficient of 0.02 was assumed and variations due to effects as tyre warming up are considered small and neglected. The value of F_N depends on the character of the road; if a motor-car climbs a gradient, $m * g * \cos \alpha$ is that part of the vehicle weight which determines the wheel pressure on the road surface, so that the rolling resistance on gradients is always lower then on level roads.

The hill-climbing resistance is given by:

$$F_h = m * g * \sin \alpha \qquad (3)$$

where

F_h	hill-climbing resistance	(N)
m	total vehicle mass	(kg)
g	gravitational acceleration	(m/s^2)
α	inclination angle	(-)

The dynamic part of the car resistance is determined by the force which is necessary to accelerate the vehicle. Resistance is experienced in accelerating the total vehicle mass in a translational sense and in accelerating the rotating parts.

The acceleration resistance may be calculated as:

$$F_a = \left[m + \Sigma I \left(\frac{i}{r}\right)^2 \right] \frac{dv}{dt} \qquad (4)$$

where

F_a	resistance due to acceleration	(N)
$\Sigma I(\frac{i}{r})^2$	the moments of inertia (I) referenced to the circumference of the driving wheel	(kg)
i	gearbox ratio	(-)
r	wheel radius	(m)

Often the sum of moments of inertia is taken in consideration with a mass factor, λ, which depends on the engaged gear, so that the momentary acceleration resistance (F_a) can be determined from the following differential equation:

$$F_a = \lambda * m * \frac{dv}{dt} \qquad (5)$$

where

λ	mass factor (1.06-1.34)	(-)

Now the total car resistance can be determined as

$$F_{tot} = \tfrac{1}{2} \rho * V_{res}^2 * A_F * C_w + m\left[g * f_r * \cos \alpha + g * \sin \alpha + \lambda * \frac{dv}{dt} \right] \qquad (6)$$

During an arbitrary driving cycle, the total energy requirement of the vehicle (W) can be determined by the following expression, if a constant drive train efficiency η is assumed in first instance:

$$W = \frac{1}{\eta} \int_0^{t_{end}} \left[F_{tot} * v \right] dt \qquad (7)$$

3. BATTERY MODEL

The battery is not only the most important part of the electric vehicle, but often the least reliable component. This is due to the fact that the amount of energy which the battery can deliver is determined by its state-of-charge. The battery state-of-charge depends upon the discharge and charge history of this energy source. During the vehicle run the state-of-charge decreases until finally the power requirements of the drive train can no longer be met. The state-of-charge is thus a crucial parameter in the calculation of the performance.

The state of a fully charged battery is well defined; however the state of a fully discharged battery depends on the discharge current: the higher the current, the lower is the available capacity. This is expressed in the empirical Peuckert relation, which states that for any current I the product

$$I^n * \tau = \text{constant} \qquad (8)$$

where

τ = time required for total discharge at current I

n = number, depending on the battery type; usually $n \approx 1.3$.

Defining C_N as the capacity at standard discharge rate (I_N) and with $C_I = I * \tau$, equation (8) can be written as

$$C_I = C_N * \left(\frac{I_N}{I}\right)^{n-1} \qquad (9)$$

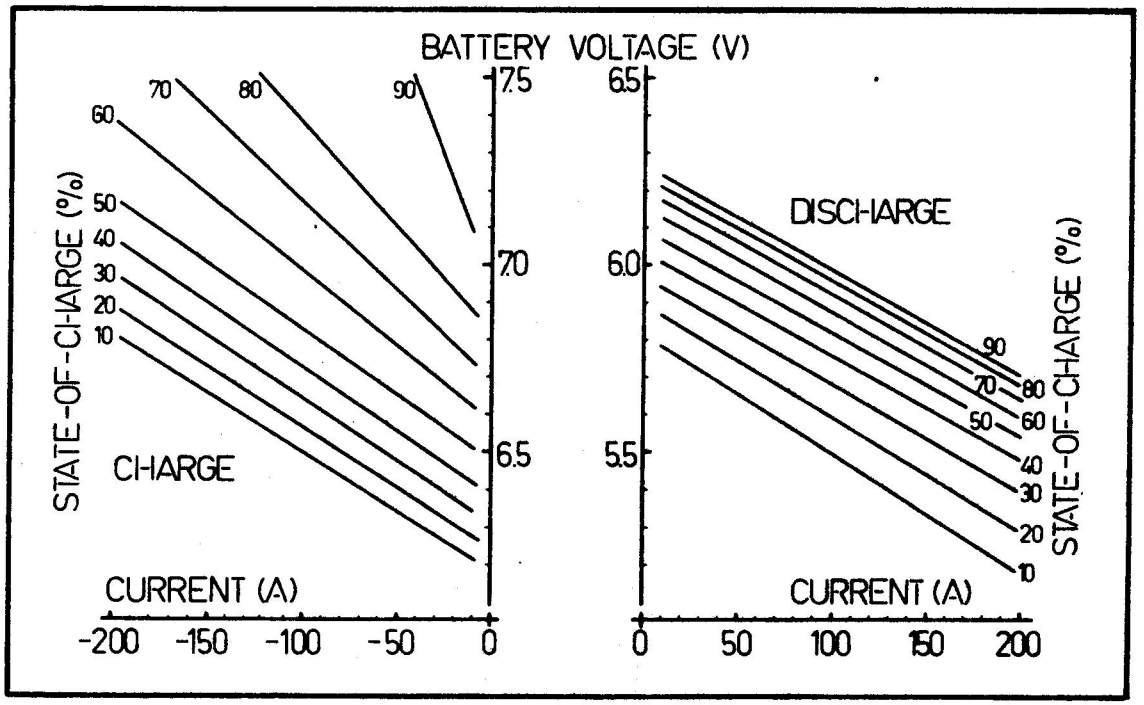

Figure 2. Voltage-current characteristics.

For electric car batteries the capacity at the 5 hr rate (C_5) is usually taken for C_N.
During discharge with current I, the state-of-charge (S) at time t can be given as [2]

$$S = 1 - \frac{I * t}{C_I} \qquad (10)$$

or with substitution of equation (9):

$$S = 1 - \frac{I * t}{C_N} \left(\frac{I}{I_N}\right)^{n-1} \qquad (11)$$

When the discharge occurs according to a duty cycle the current follows a rapidly varying pattern. The state-of-charge is then calculated for small time intervals Δt, during which I is considered to be constant:

$$S = 1 - \frac{I * \Delta t}{C_N} \left(\frac{I}{I_N}\right)^{n-1} \qquad (11a)$$

If also regenerative braking is involved in the duty cycle, then its effect on the state-of-charge must be accounted for. The incremental change of state-of-charge due to recharge with current I_c during a period Δt_c is related to the previous extent of discharge

$$\Delta S = \frac{I_c * \Delta t_c}{C_{I,d}} \qquad (12)$$

(subscripts c en d refer to charge and discharge).
With equations (9) en (11a) this can be transformed into

$$\Delta S = \frac{I_c * \Delta t_c}{I_d * \Delta t_d} (1 - S) \qquad (13)$$

When equation (13) is to be used in the case of complete recharging of a battery, a charge efficiency factor must be included because of the occurence of the water electrolysis, which becomes concurrent with the charging process during the final charging. The extent of the gassing depends on the state-of-charge and the charging current and is the predominant process for cell voltage > 2.35 Volts. For the complete recharging of a fully discharged battery the average charge efficiency factor is about 0.90.

In order to obtain more information about the charging efficiency during duty cycle operation, charge efficiency

measurements were carried out for duty cycles with and without regenerative braking. The duty cycle, which was applied, is an actual duty cycle as described earlier [3]. In these experiments the duration of the duty cycle was varied from 20 minutes (decrease of S is 6%) to 180 minutes. From the results it can be concluded that the partial recharge during a duty cycle occurs with 100% efficiency. Whether this also holds for a nearly full battery $0.94 \leq S \leq 1$ was not established, but the values of the cell voltage for recharge pulses during the initial part of the duty cycle generally do not exceed the gassing voltage even though the current during recharge can reach values of $5 * I_5$.

Experimental data of battery voltage as a function of the state-of-charge were collected from discharge and charge measurements at a 6 Volts battery (C_5 = 180 Ah).
From the voltage-time recordings at constant I (I was varied from I_5 to $5 * I_5$) voltage-current plots were constructed at constant S, as shown in Figure 2. Since the charge efficiency is not known the data in the charge plot for E > 7.25 Volts can only be indicative and refer actually to lower S.

4. MOTOR MODEL

The purpose of the motor model is to describe the motor efficiency as a function of the motor shaft output torque and speed over the entire operating range. The DC motor is actually a converter between the electrical power source and the mechanical drive train.

Several models for DC motors can be stored in the program; in this paper the model of a separately excited DC motor is discussed.
The armature controller adjusts the voltage applied to the armature of this motor and a field controller performs the same function with respect to the field.

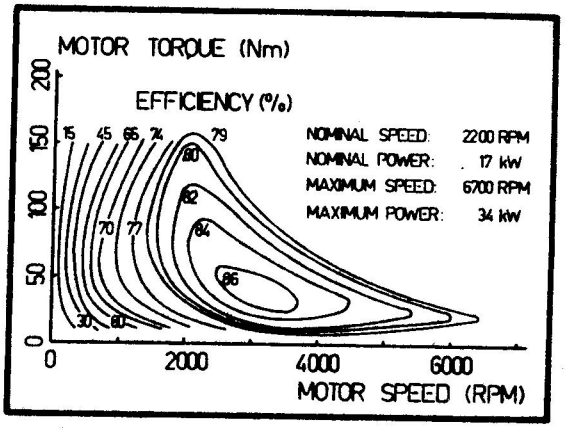

Figure 3. Motor efficiency.

For low rotation speeds of the motor the field current is kept constant and the speed is adjusted by controlling the armature voltage. With increasing rotation speed finally the full battery voltage is applied to the motor and further increase of speed is then realised by reduction of the field current. In this case the armature chopper can be bypassed which consequently results in a controller efficiency close to 100%.

The motor type is specified by

- peak power rating during three minutes
- continuous power rating
- maximum speed
- nominal speed, below which the motor operates in constant torque and above the motor operates in constant power (in connection with eventual short-circuiting of the chopper - and thus eliminating power losses in it - at speeds exceeding this number of revolutions).

The motor efficiency model is generated by using the manufacturers test data which we verified for speeds up to 3000 RPM. These motor data (Figure 3) might be stored as an efficiency table, so that the efficiency can be obtained by interpolation. This technique has not been used because of the large memory space required for a high accuracy. The motor efficiencies are represented by equations, which have been obtained by surface fitting in the form of bicubic splines.

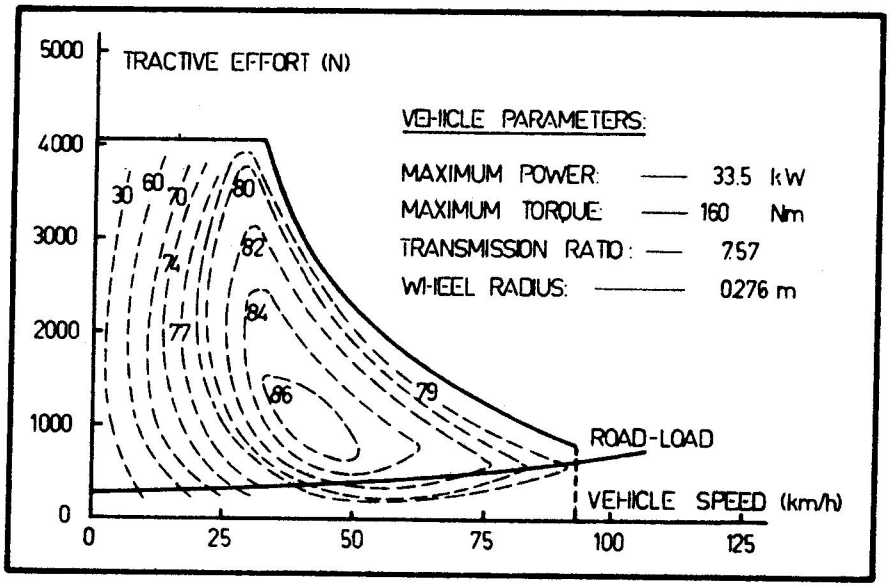

Figure 4. Vehicle characteristics; fixed gear ratio.

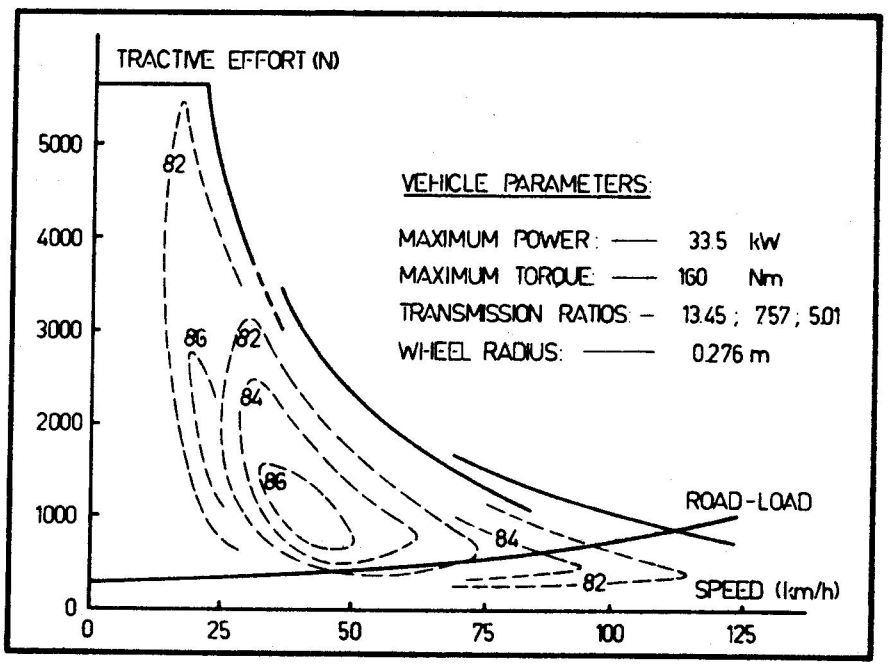

Figure 5. Vehicle characteristics; variable gear ratio.

For reasons of simplicity the same set of efficiency data is used when the machine is operating as a generator. Motor efficiency is then calculated as a function of the required output performance, which results from the driving cycle.

5. MECHANICAL TRANSMISSION

In principle a vehicle requires an infinite speed control range, because all speeds between standstill and maximum speed must be attainable. However speeds between 0 and 5 to 10 km/h are of short duration, so that a 20 : 1 control range at high efficiency is sufficient. Owing to the relatively low current requirements of seperately excited fields, field controllers are almost exclusively cheap single-quadrant transistor type controllers. Because only a 3 : 1 control range is realised by field weakening, further adjustment is necessary by variation of the armature voltage and/or variable transmission ratios.

If the separately excited motor is controlled continuously by an armature chopper and a field controller, every point within the torque-speed envelope can be adjusted and an infinite control range is realised; consequently a fixed gear ratio is sufficient (Figure 4). Because separately excited motors are less efficient at low speeds, a manual or automatic gear drive may be attractive, because these gears allow highly efficient motor operation. Figure 5 shows the propulsion characteristics of the motor in combination with 3 speeds of a manual gearbox. Another advantage of this propulsion system is that in this case the armature controller is not required. However the disadvantages of this system are reduced driving comfort and operatibility: a fully electronic system permits completely yerk-free acceleration and driving without gear change. It may be noticed that the behaviour of the former propulsion system is exactly the same as that of an ICE-vehicle with a normal gearbox.

Usually motor-car manufacturers assume a fixed gearbox efficiency (95 to 97%). In case of propulsion by internal combustion engines the gearbox efficiency is of small importance, because transmission losses are small in comparison with ICE losses, although even this statement is disputable. With respect to the relatively small amount of stored energy in the electric car particular attention has to be paid to losses in the electric vehicle gears. The losses in these components are functions of both speed and load again. The total loss of power is due to two main causes; (i), the viscous resistance due to gear-wheel churning in the lubricant and friction in bearings and seals and, (ii), the friction between the sliding teeth of the gears. The former is independent of and the latter dependent on the load transmitted, The tooth friction is practically unaffected by changes of speed.

From efficiency measurements at the Eindhoven University curves at constant efficiency have been constructed for a 4-speed manual transmission, including differential, as it is used in the european VW Rabbit 1600 (Figure 6). The measured efficiencies are relatively high because a helical gear type final drive has been integrated with the transmission instead of the usually seperate bevel gear final reduction. In the simulation model these efficiency characteristics are represented by equations, using surface fitting with bicubic splines. Increases in efficiency due to effects as gear lubricant warming up were considered small and therefore neglected. It is planned to extend the program by a model for an automatic 3-speed planetary gearbox by the end of this year.

6. ELECTRIC VEHICLE SIMULATION

The principle of a drive train simulation is to calculate the power-flow through this train during a specified duty cyle in which the vehicle speed has been

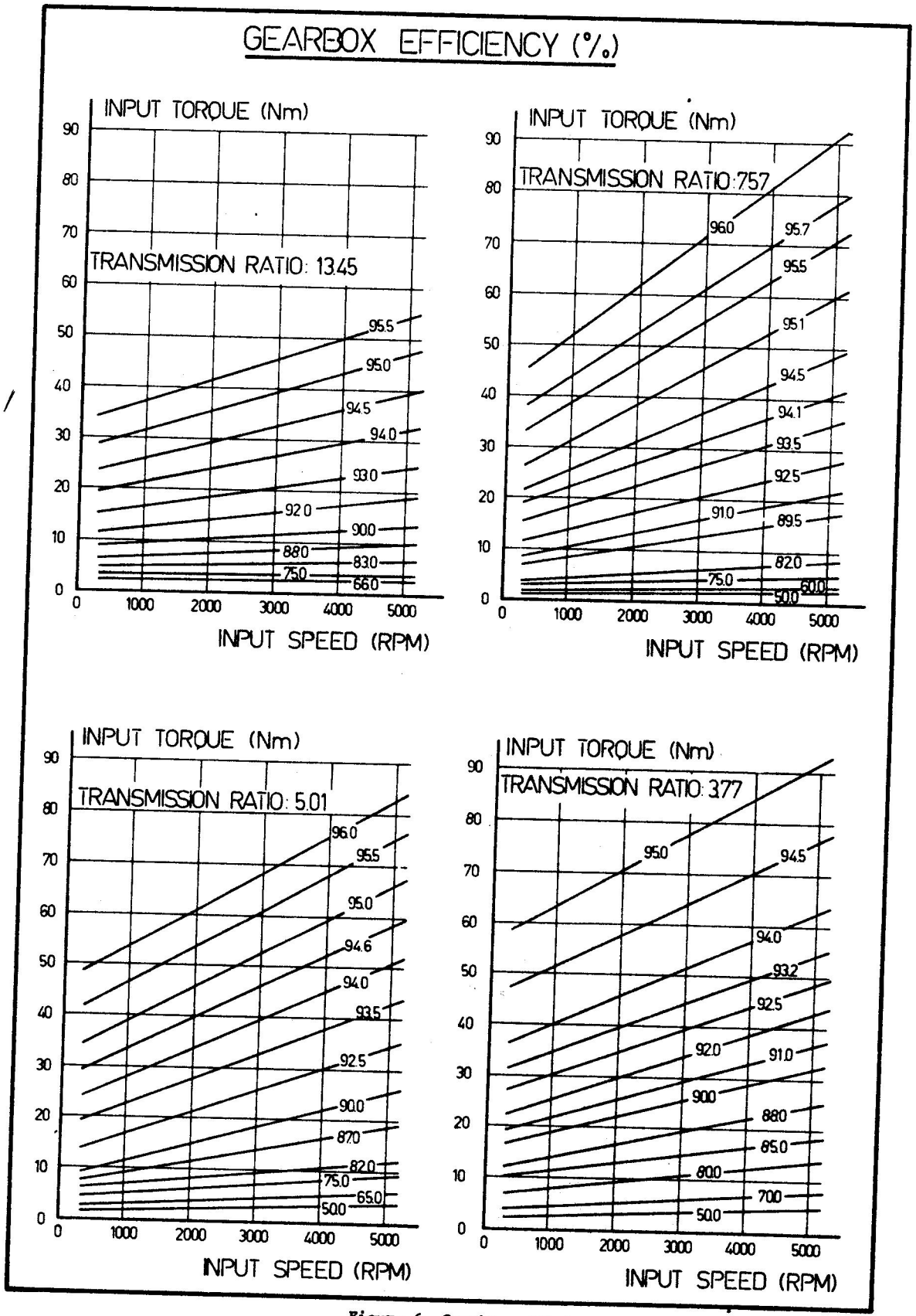

Figure 6. Gearbox efficiency.

prescribed as a function of time. Starting with the wheel power requirements the power flow is calculated from the wheels through the gears, motor and electronic controllers to the battery for a sequence of speeds constituting the total driving cycle. Regenerative braking has been included.

The input variables of the computer program by which the simulation is carried out comprise the characteristics of vehicle, transmission, motor, controller, battery and driving cycle and have been listed in Table I. The flow-chart, given in Figure 7, represents the sequential and logical structure of the program.

From the characteristics of motor, transmission and battery, as discussed in previous chapters, the conditions and each operating point can be calculated by means of subroutines.

It has been assumed that the battery can deliver the required power until a determined minimum cell voltage is reached where the battery is declared to be fully discharged. In the same way regenerative braking is not permitted above a maximum charging voltage, related with "gassing" voltage. In this case the battery may only be charged by a current, which is allowed by this voltage and the power remainder is assumed to be dissipated in the mechanical brakes.

The output of the simulation provides numerical values for e.g.: instanteous tractive effort, conditions of transmission, motor and battery and cumulative energy used and distance covered. These are shown in Figures 8 and 9.

If during motoring or regenerative braking a drive situation requires a motor speed and/or torque exceeding the limits of the motor data, the program excecution terminates. The program has been built up in a modular way, so that it can easily be adapted for other types of components and/or drive lines.

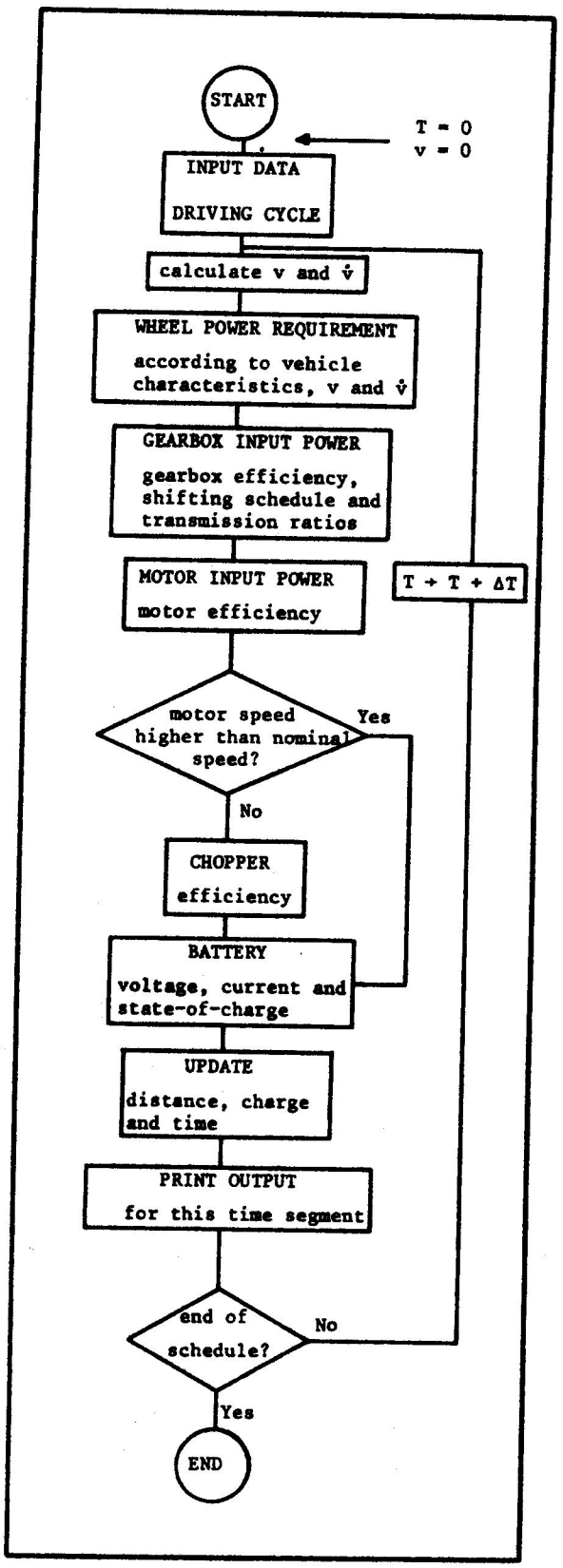

Figure 7. Simulation flow-chart.

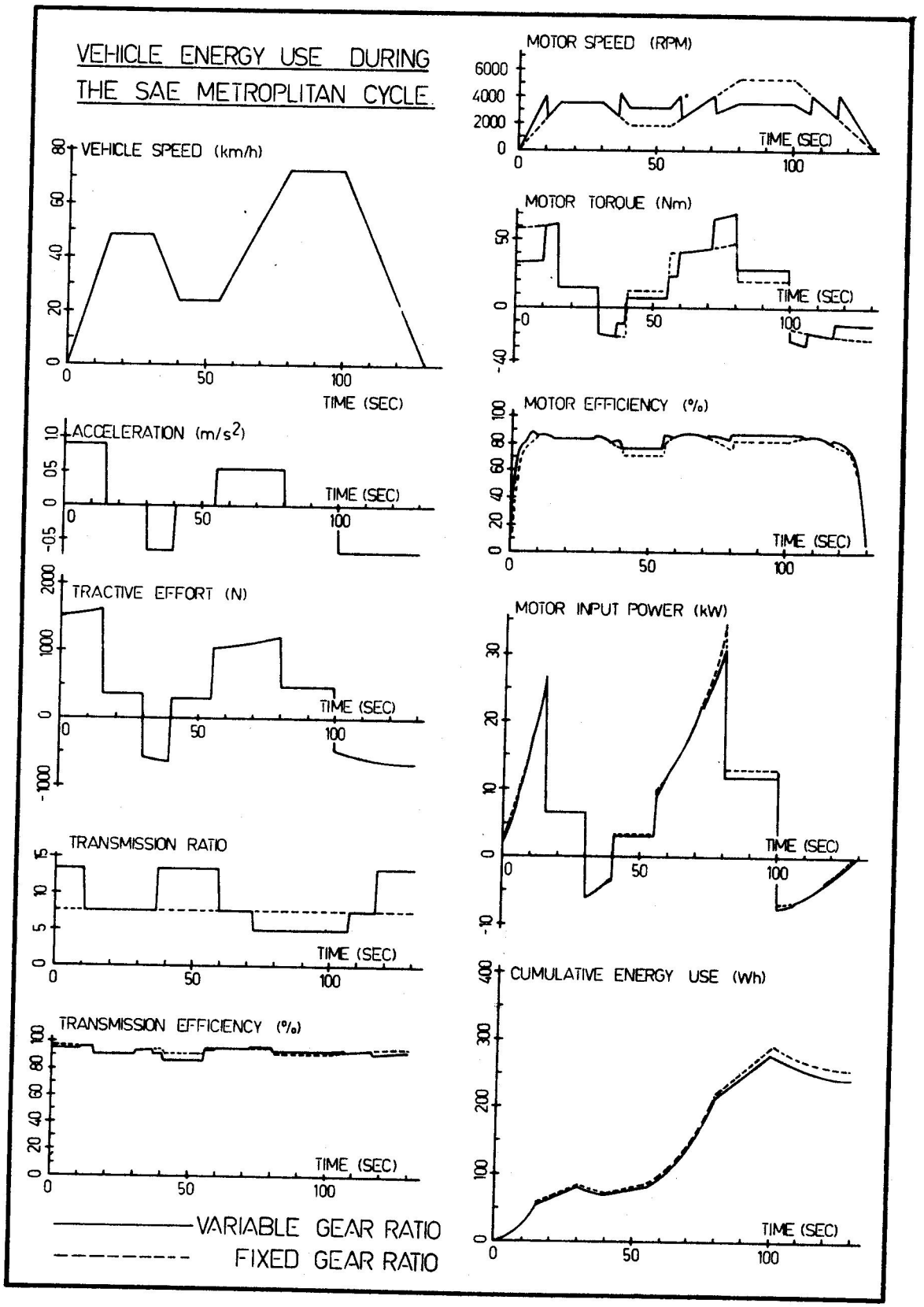

Figure 8. Vehicle energy use on driving cycle.

VEHICLE	MOTOR	BATTERY
. weight . frontal area surface . aerodynamic drag coefficient . rolling resistance coefficient . wheel radius	. maximum power . nominal power . maximum speed . nominal speed . efficiency map	. discharge capacity at 5 hour rate . nominal voltage . maximum voltage . minimum voltage . voltage characteristics as function of current and state-of-charge . charge efficiency
TRANSMISSION	**CONTROLLER**	**DRIVING CYCLE**
. efficiency maps . transmission ratios . shifting schedule	. efficiency	. arrays of velocity-time pairs . time step Δt

Table 1. Input parameters for EV simulation.

7. RESULTS AND CONCLUSIONS

The described computer simulation has been applied to an electric vehicle following the SAE J227 Metropolitan Cycle. Although other cycles can easily be used this cycle has been chosen because it concerns a short driving schedule with variety of speeds. The test vehicle is a completely modified Volkswagen Rabbit, equipped with a separately excited DC motor and a fully electronic motor control, which allows regenerative braking. The complete specifications are given in Table 2.

The battery pack consists of 24 lead-acid batteries of 6 Volts each. The end of the operating range was declared to be reached when the battery is unable to meet the power demand at any value of battery voltage above the minimum, which has been fixed at 120 Volts. In connection with gassing the maximum battery pack voltage has been specified at 174 Volts. For applying these criteria accurate simulation of the battery voltage, including cumulative battery charge reduction is of vital importance over the entire operating range.

Figure 8 shows interesting output variables of the vehicle - using a manual gearbox and a fixed gear ratio - for the Metropolitan Cycle.

In order to obtain an as efficient as possible motor operating the shifting schedule is defined in such a manner that motor speeds are kept between 2500 and 4000 RPM. This highly efficient motor operation results in a low cumulative energy use.

vehicle weight	1400.00 kg
rolling resistance coefficient	0.02 -
frontal surface area	1.80 m^2
aerdodynamic drag coefficient	0.42 -
wheel radius	0.276 m
max. motor output power	33.50 kW
max. motor output torque	160.00 Nm
battery pack:	
. nominal voltage	144.00 V
. nominal capacity at 5-hour rate	180.00 Ah
motor efficiency according to Figure 3	
transmission efficiency according to Figure 6.	

Table 2. Vehicle specifications.

In the course of the battery discharge the voltage required to provide a certain power decreases and consequently the current increases.

Energy use of SAE Metropolitan Cycle		PROPULSION TRAIN			
		1. 3-speed manual gearbox	2. fixed gear ratio: 7.57	3. fixed gear ratio: 5.01	4. fixed gear ratio: 3.77
motor speed	(RPM)	2500-4000 90% of time	0-5300	0-3500	0-2600
energy requirement at motor terminals	(Wh/tkm)	112.4	119.2	118.2	128.4
av. motor efficiency	(%)	80.70	77.88	76.67	73.56
av. transmission efficiency	(%)	92.54	93.08	94.52	93.99
av. drive train efficiency	(%)	74.68	72.49	72.47	69.14
max. motor input power	(kW)	31.0	34.5	31.0	30.8
max. motor output torque	(Nm)	70.0	61.4	91.9	123.6
operating range	(km)	85.6	73.3	81.0	74.8
discharged ampere-hours		101.94	92.21	101.66	101.50
average current	(A)	50.7	53.6	53.5	57.8

Table 3. Simulation results;different propulsion trains.

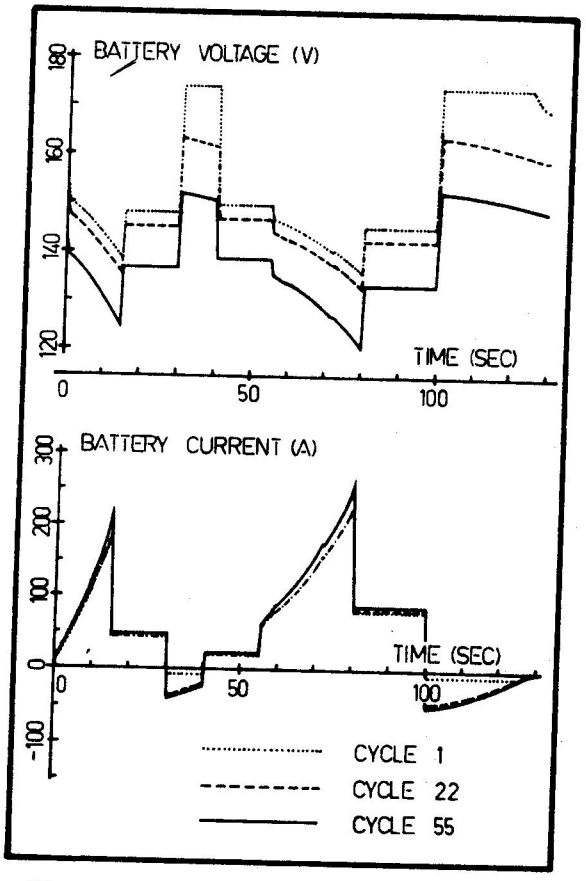

Figure 9. Battery voltage and current on SAE Metropolitan Cycle.

Battery voltage and current obtained by simulation of the first, twenty-second and fifty-fifth cycle of the vehicle with a variable gear ratio are shown in Figure 9. At the end of the second acceleration period, where the required power reaches a maximum value, the battery voltages are 135, 132 and 120.5 Volts respectively.

Table 3 shows the comparison of these drive trains with two alternative trains using a fixed gear ratio. Propulsion train 4 uses an extremely low transmission ratio, resulting in a poor motor efficiency. That is precisely the reason why the energy requirement at the motor terminals is relatively high. The average drive train efficiencies of alternatives 2 and 3 stand at 72.5% both, with consequently approximately equal motor input energy requirements. However the peak power requirement of propulsion train 2 is relatively high because a lower instantaneous drive train efficiency coincides with the maximum wheel power requirement.

Because of this higher peak power the specified minimum battery voltage is reached sooner, which results in a smaller operating range.

It may be concluded that:

- from an energetical point of view a propulsion train using a variable transmisson ratio has to be preferred to a drive system with a fixed gear ratio.
- the operating range depends on both peak power requirement and average energy requirement per kilometer; so power train optimizing with respect to the peak power demand is strongly recommended.
- this simulation program allows an accurate comparison of vehicle drive trains while component deficiencies are obviously demonstrated.

REFERENCES

1. van Dongen, L.A.M., "Propulsion of Electric Vehicles - Matching Components to the Energy Requirements of the Vehicle", Electric Vehicle Developments, No. 8, December 1980, pp 17-22.

2. White, K.E., "A Digital Computer Program for Simulating Electric Vehicle Performance", Society of Automotive Engineers, paper 78216, pp 1-14.

3. Visscher, W.H.M., de Zeeuw, W. and van der Graaf, R.,"Experiments on Lead-Acid Batteries for an Electric Vehicle", Proceedings of the Fifth International Electric Vehicle Symposium, No. 783107, pp 1-10.

4. Nelson, R.H., Jacovides, L.J., Schauerte, F.J. and Woods, E.J., "Electric Vehicle Simulation Program", Proceedings of the Fifth International Electric Vehicle Symposium, No. 782207, pp 1-11.

5. Bader, C. and Stephan, W., "Comparison of Electric Drives for Road Vehicles", IEEE Transactions on Vehicular Technology, Vol. VT-26, No. 2, May 1977, pp 123-128.

6. Murphy, G.J., "Alternative Approaches to Speed Control in Electric Vehicles", Society of Automotive Engineers, paper 780292, pp 1-11.

BATTERY STATE OF CHARGE MODEL FOR DRIVING CYCLE OPERATION

W. Visscher and L. van Dongen, Eindhoven University of Technology,
P.O. Box 513, 5600 MB Eindhoven, The Netherlands.

ABSTRACT
The actual performance of an electric vehicle depends on the capability of the battery to meet the power requirements of the drive train. In order to predict the vehicle operating range an accurate battery model is required. The behaviour of a battery depends on its state of charge. In the definition of the state of charge the characteristic relationship between available capacity and current must be accounted for.
A voltage-current relationship is derived based on the polarization behaviour of a lead acid battery. This equation expresses the battery voltage as a function of current and state of charge. The theoretical equation is verified with data experimentally established at a 6 V. battery. A program is written that calculates the cumulative charge reduction during driving cycle operation. This gives the state of charge as the driving cycle proceeds. By combining this with the relationship between voltage, current and state of charge, the battery voltage during the total driving cycle can be determined.
Battery voltage and energy are thus calculated for several types of driving cycles. These results will be compared with experimental data at a 6 V. battery.

1. INTRODUCTION

The actual performance of an E.V. depends on the capability of the battery to meet the power requirements of the drive train. Operating modes differ widely and the vehicle characteristics vary with each model. Therefore, normalized drive cycles were proposed based on analysis of traffic patterns and several duty cycles are now in use to test battery performance for a given type of vehicle. Several attempts have been made to give also a model for the battery. Due to the chemical and physical processes that occur in the battery, its behaviour is more difficult to describe by an accurate model; moreover the battery characteristics change with time.
With models for the components of the drive train and the battery, computer simulation can be carried out to study the interaction of battery and drive train and to predict energy use, vehicle performance and operating range.
This paper will describe a battery model and compare calculated state of charge values with experimental data.

2. THE STATE OF CHARGE

The amount of energy that the battery can deliver is determined by its current-voltage characteristic which in turn depends upon the state of charge.
The state of charge of a fully charged battery is well defined; the concept of complete discharge depends on the discharge current due to the fact that in a battery the available capacity decreases with higher current. Hence the state of charge (S) at time t during discharge with current I must be related to the capacity (C_I) at current I [1]

$$S = 1 - \frac{I\ t}{C_I} \qquad (1)$$

With the Peuckert relation

$$I^n * \tau = \text{constant} \qquad (2)$$

where τ = time required for complete discharge at current I
n = number, depending on the battery type, $1.2 < n < 1.4$

C_I can be expressed in the capacity (C_N) at standard rate (I_N)

$$C_I = C_N \left(\frac{I_N}{I}\right)^{n-1} \qquad (3)$$

The state of charge at any current is then related to the standard capacity with

$$S = 1 - \frac{It}{C_N}\left(\frac{I}{I_N}\right)^{n-1} \qquad (4)$$

3. BATTERY DISCHARGE MODEL

Mathematical models for porous electrodes have been developed to describe the extent of utilization of a battery plate as a function of rate of discharge, involving structural changes during the discharge process [2,3,4,5]. These are derived from the kinetic relationship between current density and electrode potential, taking into account mass transfer processes.
The complete battery behaviour is often described by the current-voltage relationship of Shephard [6]

$$E = E_s - K\frac{Q}{Q - It} - R_E I \qquad (5)$$

in which
K = polarization parameter
Q = amount of available active material
R_E = electrolyte resistance
E_s = constant voltage.

This equation has been derived assuming a linear relationship between current and potential at both electrodes. However, such a behaviour is a priori restricted to very low polarization conditions. Moreover, to fit the experimental data with eq. (5) a negative value of the resistance had to be chosen. This inconsistency was recognized by Shephard and attributed to the empirical nature of the equation.

During discharge with electric vehicle duty cycles high polarization conditions will prevail. Therefore a current-voltage relation will be derived which is applicable to high current discharge.

At the two electrodes 1 and 2 of the battery the discharge process takes place via cathodic reaction at electrode 1 and anodic reaction at electrode 2; this can be expressed by the general electrochemical rate equations

at electrode 1 : $p\ OX_1 + ne^- \rightarrow p'\ RED_1$
at electrode 2 : $q\ RED_2 \rightarrow q'\ OX_2 + ne^-$

where OX_1 and RED_2 stand for the concentration of dissolved species at electrode 1 and 2 respectively.
p, p', q, q' = stoichiometric coefficients
n = number of electrons

At the two electrodes of the Pb acid battery these processes are:
at electrode 1 : $PbO_2 + 3\ H^+ + HSO_4^- + 2\ e^- \rightarrow PbSO_4 + 2\ H_2O$
at electrode 2 : $Pb + HSO_4^- \rightarrow PbSO_4 + H^+ + 2\ e^-$.

Under the conditions that the electron transfer occurs rapidly and that mass transfer to and in the pores of the electrode limits the rate of the reaction, the overpotential (η) for the reaction at electrode 1 is given by

$$\eta = \frac{RT}{nF} \ln \left(\frac{c_{OX,t}}{c_{OX,t=0}} \right)^{p} \qquad (6)$$

and similarly at electrode 2

$$\eta = - \frac{RT}{nF} \ln \left(\frac{c_{RED,t}}{c_{RED,t=0}} \right)^{q} \qquad (7)$$

where: η = overpotential [V]
R = gas constant [J.mol^{-1} K^{-1}]
T = absolute temperature [K]
F = Faraday constant [C mol^{-1}]
n = number of electrons

For a battery plate the concentration term $c_{OX,t=0}$ can be considered to be equivalent to the total amount of charge that is available at the fully charged plate 1, whereas $c_{OX,t}$ is the charge remaining after discharge with current I during time t, so

$$c_{OX,t} = c_{OX,t=0} - It \qquad (8)$$

With $C_{I,1}$ = capacity of electrode 1 at current I we have

$$\frac{c_{OX,t}}{c_{OX,t=0}} = 1 - \frac{It}{C_{I,1}} \qquad (9)$$

i.e. $\frac{c_{OX,t}}{c_{OX,t=0}}$ represents the state of charge $S_{I,1}$ of electrode 1.

Similarly $\frac{c_{RED,t}}{c_{RED,t=0}} = S_{I,2}$ for electrode 2.

The total cell voltage (E) during discharge is given by the algebraic sum of the two electrode polarizations:

$$E = E_{eq,1} + \eta_1 - (E_{eq,2} + \eta_2) - I R_E \qquad (10)$$

in which $E_{eq,1,2}$ = equilibrium potential of the electrode reaction 1, respectively 2
R_E = electrolyte resistance.

If both electrodes have the same capacity $C_{I,1} = C_{I,2}$ then $S_1 = S_2 = S$ and we can write for eq. (10) with substitution of (6), (7), (9)

$$E = E_{s=1} + \frac{(p+q)}{2} \frac{RT}{F} \ln S - I R_E \qquad (11)$$

where $E_{s=1} = E_{eq,1} - E_{eq,2}$

i.e. the cell voltage of a fully charged battery and determined by the H_2SO_4 concentration.
The electrolyte resistance R_E is in principle a function of the state of charge.

Eq. (11) describes the cell voltage during discharge with current I in dependence of the state of charge. It should be noted that this equation is restricted to high polarization conditions and hence is not valid at very low current or at I = 0.

To establish the parameters of eq. (11) discharge curves were recorded at a Pb acid battery at various I. The battery was a Varta electric vehicle battery, 6 V, type 240-15 with nominal capacity C_5 = 180 Ah. Capacity measurements as function of I gave a value of n = 1.26 for the Peuckert relation (2).
After each discharge the battery was charged with 20 A and finally with 6 A until the specific gravity was constant. From the data E-I plots were constructed at constant S, with S calculated according to eq. (4). This is represented in Fig. 1.

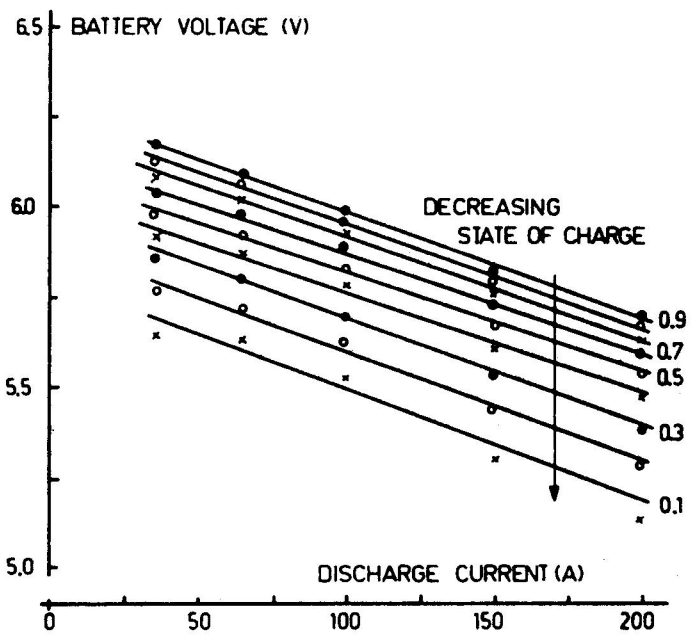

Fig. 1. Voltage-current characteristic during discharge as a function of state of charge.

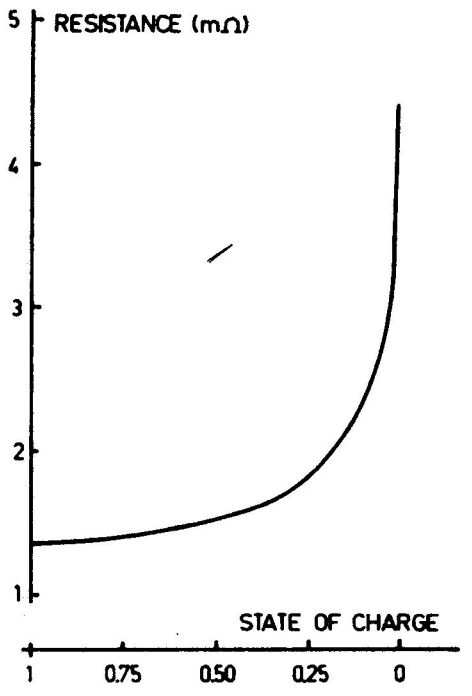

Fig. 2. Electrolyte resistance of 6 V battery for decreasing state of charge.

Fig. 2 shows the electrolyte resistance as a function of the state of charge measured by discharging the battery at C_5 rate to decreasing states of charge.
When the results of Fig. 1 are represented as a plot of E vs. ln S (Fig. 3) a linear relationship is obtained and the slope of the curves is independent of the current. This is in agreement with eq. (11). The observed slope was found to be 0.26 V. About the same value was found when voltage - state of discharge plots given by Schleuter [7] for a tubular battery were replotted.
Fig. 2 shows that R_E does not vary significantly for $1 > S > 0.6$, so from eq. (11) it would follow that the slope of the E-I plot for high S is independent of S and is equal to R_E.
Though the experimental lines are indeed parallel, the slope is about $2 \times R_E$. (At S = 1 R_E = 1.37 mΩ). This can be explained by the resistance of the electrolyte in the pores which is not measured during steady state experiments of Fig. 3 but will contribute during actual discharge.

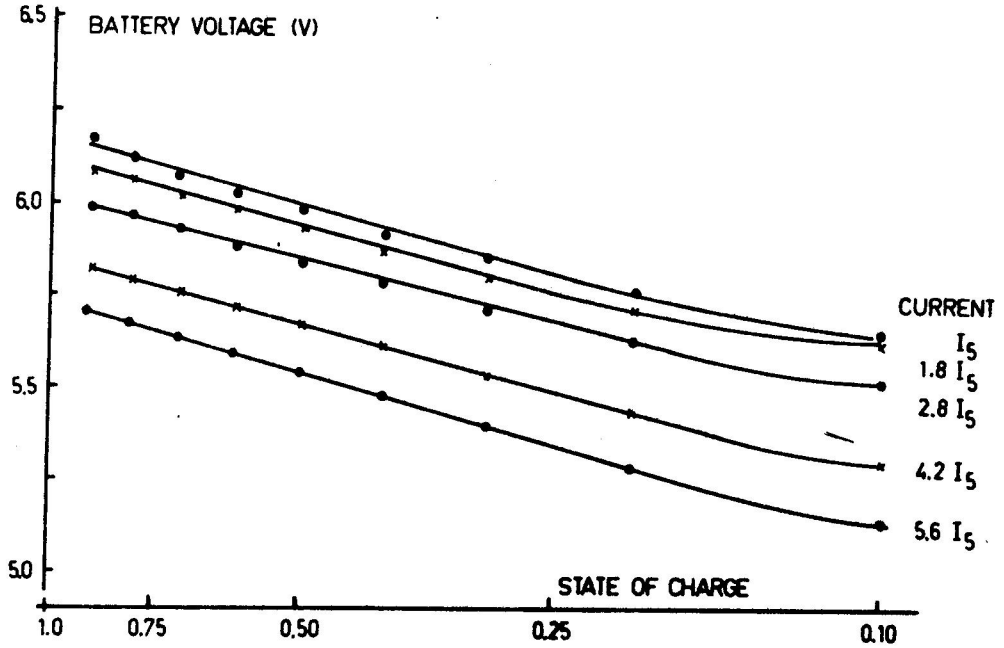

Fig. 3. Battery voltage vs. state of charge.

The above results show that the discharge behaviour at high polarization can indeed be described by a rather simple relationship.

4. STATE OF CHARGE OF THE BATTERY DURING DUTY CYCLE OPERATION

4.1. Model.

When the discharge of a battery takes place along the pattern of a duty cycle, the current changes rapidly, moreover regenerative braking is involved. To account for this the state of charge must be calculated for small time intervals Δt during which I is considered to be constant, hence during discharge:

$$S = 1 - \frac{I\ \Delta t}{C_N} \left(\frac{I}{I_N}\right)^{n-1} \qquad (12)$$

whereas during charge the incremental change of state of charge (ΔS) during a period Δt_c is given by [1]

$$\Delta S = \frac{I_c\ \Delta t_c}{C I_d} \qquad (13)$$

or with (2)

$$\Delta S = \frac{I_c\ \Delta t_c}{I_d\ \Delta t_d} (1-S) \qquad (14)$$

(Subscript c, d refers to charge respectively discharge).
A computer program was written to calculate the state of charge with eq. (11) and (13) after discharge with a given duty cycle, using the experimentally established E-I curves at constant S. The program calculates also the cell voltage and current during the duty cycle.

4.2. Battery power schedules.

These simulation results were compared with the actual battery performance during duty cycle operation. The load cycle experiments were carried out at a 6 V battery with a machine convertor, consisting of an induction machine coupled to a 20 V - 400 A d.c. machine [8].

The total battery requirement of a vehicle following a velocity profile was calculated for the vehicle being built by the Eindhoven Electric car group. The main drag forces to be overcome are given by

$$F_{st} = f_r\ g\ M + \frac{1}{2}\ \rho\ C_x\ A\ v^2 \qquad (15)$$

where the parameters have the following meaning and specific value:

F_{st}	= drag force due to tire hysterisis and wind resistance	[N]
f_r	= coefficient of rolling resistance	(0.02)
g	= gravitational acceleration	(9.82 m s^{-2})
M	= vehicle mass	(1350 kg)
ρ	= air density	(1.29 kg m^{-3})
C_x	= aerodynamic drag coefficient	(0.42)
A	= frontal surface area of the vehicle /	(1.80 m^2)
v	= vehicle speed	[m s^{-1}]

Substitution of these values in eq. (15) gives

$$F_{st} = 264.87 + 0.488\ v^2 \qquad (16)$$

The total tractive effort of the vehicle (F_t) is equal to:

$$F_t = F_{st} + F_a = 264.87 + 0.488\ v^2 + M\ a \qquad (17)$$

F_a	= accelerating force	[N]
a	= vehicle acceleration	[m s^{-2}]

The wheel power requirement (in Watt) can be represented as

$$P = [264.87 + 0.488\ v^2 + M\ a]\ v \qquad (18)$$

Starting from this equation, the battery power has been determined assuming the average motor and gearbox efficiency to be 80 and 90% respectively.
The battery behaviour was investigated during three types of duty cycles viz. the European cycle, the SAE J 227 aD cycle and the T.H.E. cycle. The first two cycles are standard velocity versus time profiles; Fig. 4 and 5 show the power profiles, calculated for the total battery pack (144 V). (See page 7).

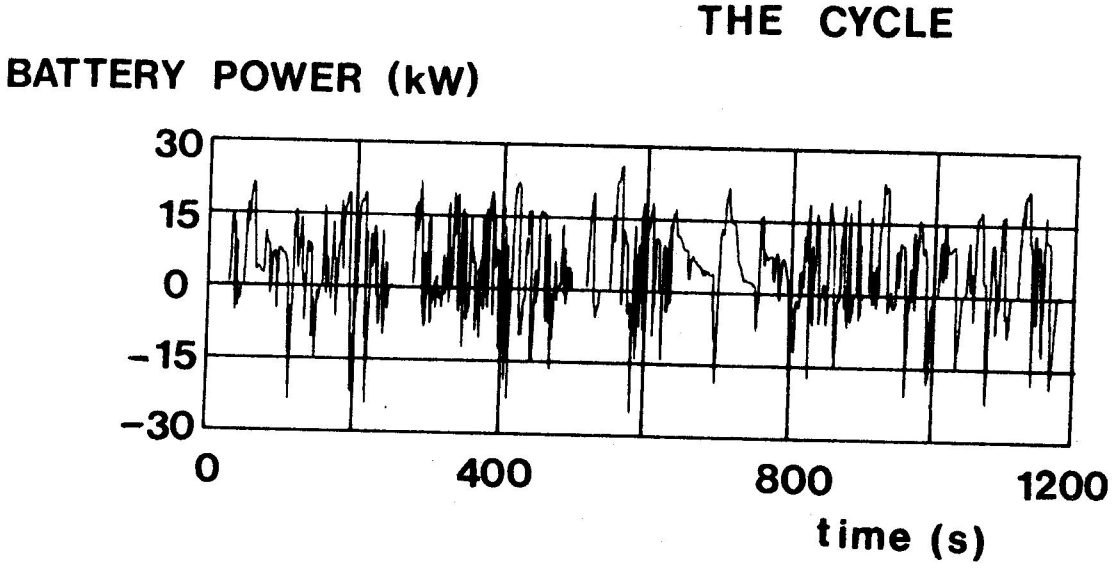

Fig. 6. Battery power for THE duty cycle.

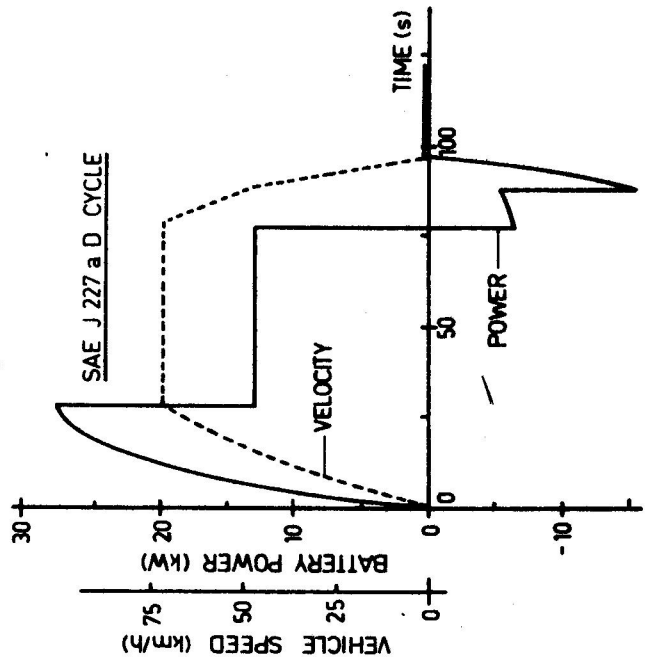

Fig. 5. Battery power and vehicle speed for SAE J 227 aD duty cycle.

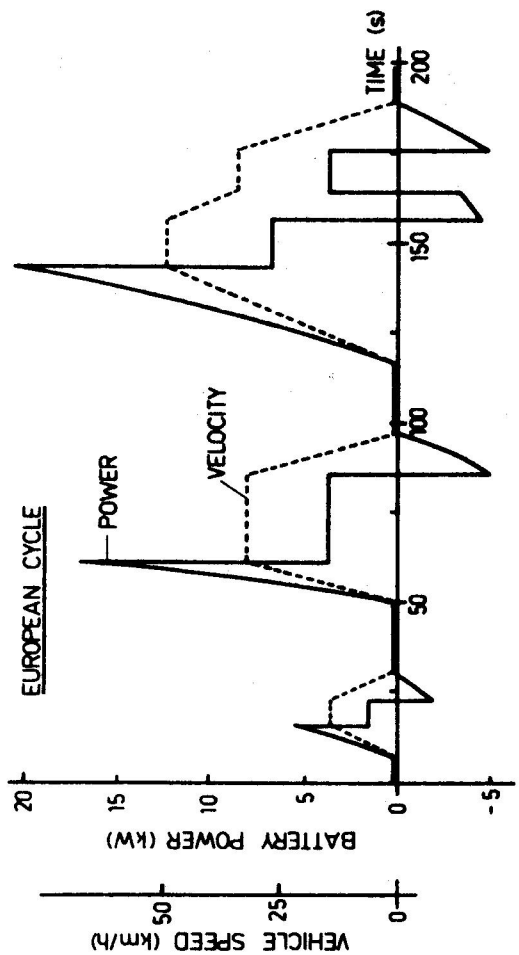

Fig. 4. Battery power and vehicle speed for European duty cycle.

The THE cycle was chosen as a representative of actual duty cycles, which have been recorded in typical Dutch cities with the aid of a DAF 31 outfitted with speed sensors and torque transducers at the rear wheel axles. Conversion of the results with respect to the estimated mass and drive train efficiency of the Eindhoven Electric Vehicle resulted in the battery power for the total battery pack profile indicated in Fig. 6. The duration of one cycle is 20 minutes in contrast with the usually shorter cycle time of the standard duty cycles.
Table 1 summarizes some duty cycle specifications.

	EUR.	SAE J 227 aD	THE
Average vehicle energy [Wh/km]	145	189	140
Average vehicle speed [km/hr]	18.3	44.7	24.3
Distance covered per cycle [km]	1.010	1.516	8.1
Duration of 1 cycle [s]	198	122	1200
Stops/km	3	0.66	9
Idling time [%]	29.3	20.49	10.54
$\frac{\text{Charge recuperation}}{\text{total discharge}}$ [%]	19.4	10	22.2

Table 1. Duty cycle specifications.

4.3. Voltage-current characteristics.
E-I diagrams at constant S for the charging process were obtained from constant charging curves at various I starting with a battery discharged to S = 0 with I_5. The results, given in Fig. 7, represent only the E-I curves for which the charge efficiency is 100%. Due to concurrent water electrolysis, the charge efficiency becomes less than 100% for E $\geq$ 2.35 V per cell. To account for this in eq. (13) the charge efficiency factor must be introduced and E-I plots for S > 0.6 will be presented later.

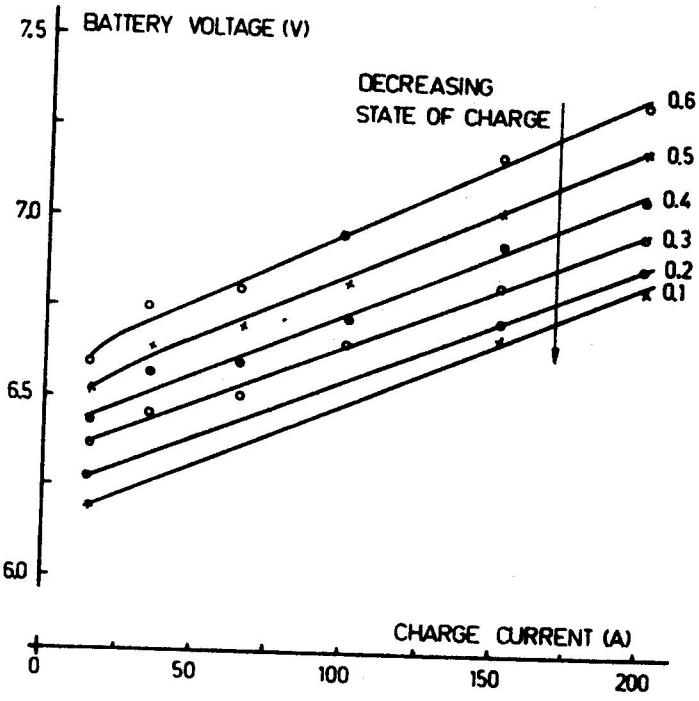

Fig. 7. Voltage-current diagram during charging as a function of state of charge up to S = 0.6.

4.4. Comparison of test- and simulation results.

The European and SAE J 227 aD cycle tests.

To avoid the voltage range where charging might be inefficient, the calculation of the battery performance during the European and the SAE J 227 aD duty cycle was started at S = 0.6. This was experimentally realized by discharging the battery (Varta electric vehicle battery 6 V, 240.15 nominal capacity C_5 = 180 Ah), during 2 hr at C_5 rate. The battery was then subjected to a number of cycles (European or SAE) and thereafter the rest capacity (C_R) was measured at the C_5 rate.

Results:

	Experimental	Calculated
European cycle		
Netto discharge during 60 cycles (Ah)	59.8	63.1
C_{Rest} (Ah)	36.0	35.1
SAE J 227 aD cycle		
Netto discharge during 30 cycles (Ah)	65.5	66.5
C_{Rest}	24.0	13.8

The experimental and calculated voltage and current profiles during the 60th European cycle and during the 30th SAE cycle are given in Fig. 8 and 9 respectively.

The battery voltage during discharge agrees within 0.1 V with the computed value but the experimental data during charging are lower, indicating a retarded battery respons such that very rapid current changes are less effective.

Calculation of the state of charge shows that S = 0 will be reached after 55 SAE cycles, i.e. an operating range of 83 km. This is in agreement with the experimental observation that the discharge could be continued during about 53 cycles before the power delivered by the battery at the highest discharge peak was 10% less than demanded by the duty cycle.

THE cycle tests

The average current of the THE cycle is ca. 33 A, the maximum current during discharge is ca. 200 A, during charge 160 A.
The battery could meet the duty cycle demands during 13 cycles (i.e. operating range 105.3 km).
After the battery had been discharged with 13 cycles C_R was determined at C_5 rate. The experimental C_R was found to be 31 ± 5 Ah, while the calculated C_R was 19.2 Ah.
Fig. 10 shows the cell voltage (E_D) at the highest discharge peak and the cell voltage (E_C) at the highest charge current peak during 13 cycles and the cell voltage E_R at I = 0 at the end of each cycle. In the figure the computed data are given from 8th to 13th cycle.

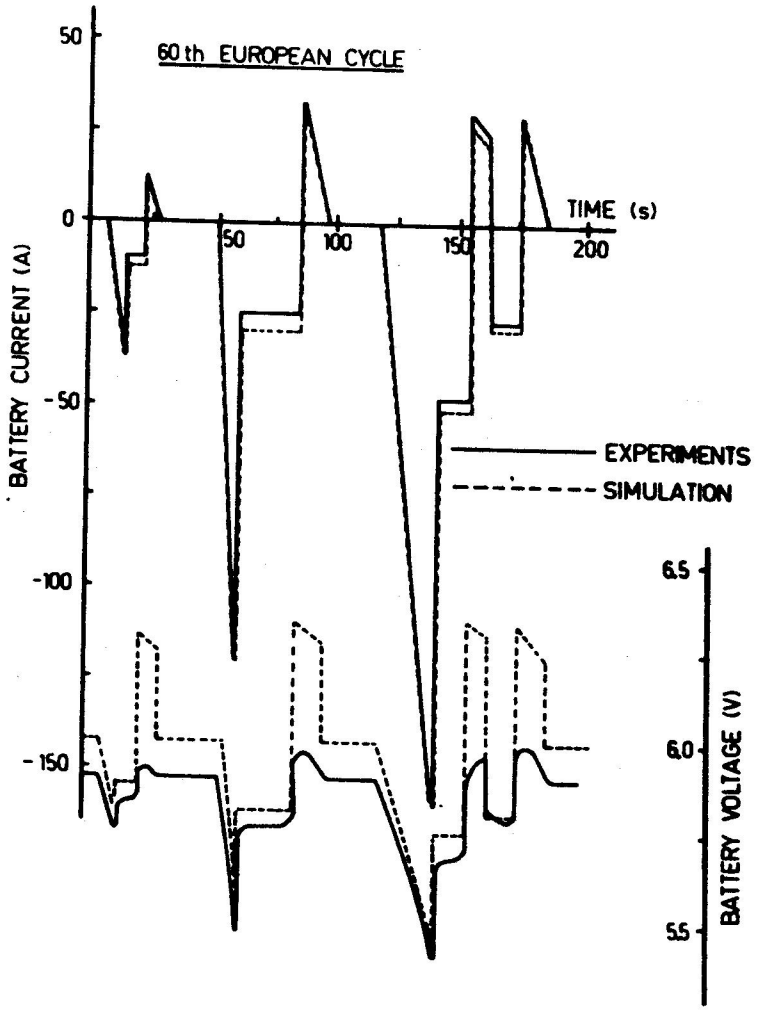

Fig. 8. Simulated and experimental battery voltage and current profile during 60th European cycle.

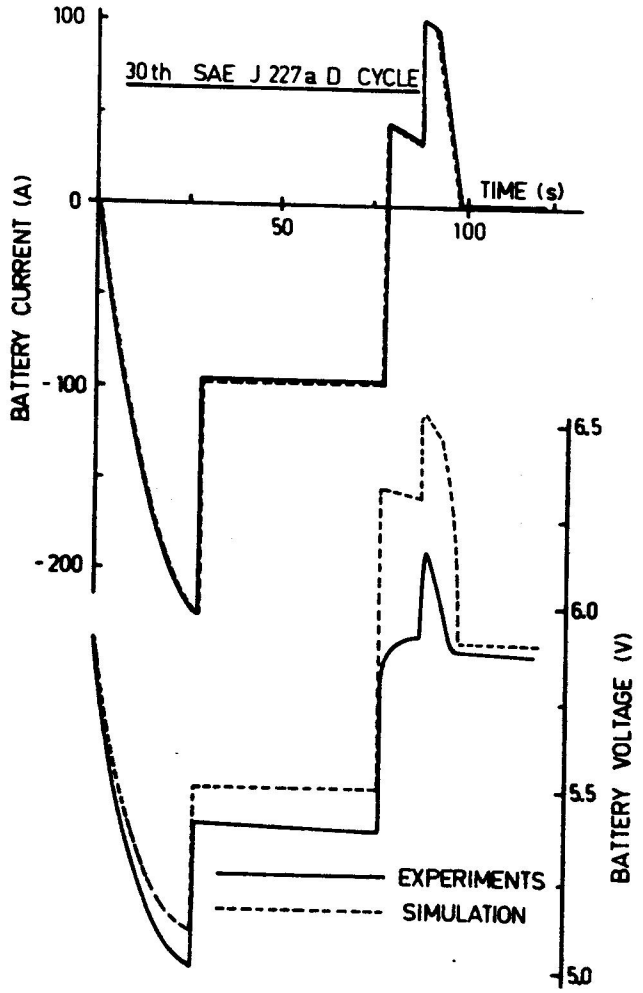

Fig. 9. Simulated and experimental battery voltage and current profile during 30th SAE J 227 aD cycle.

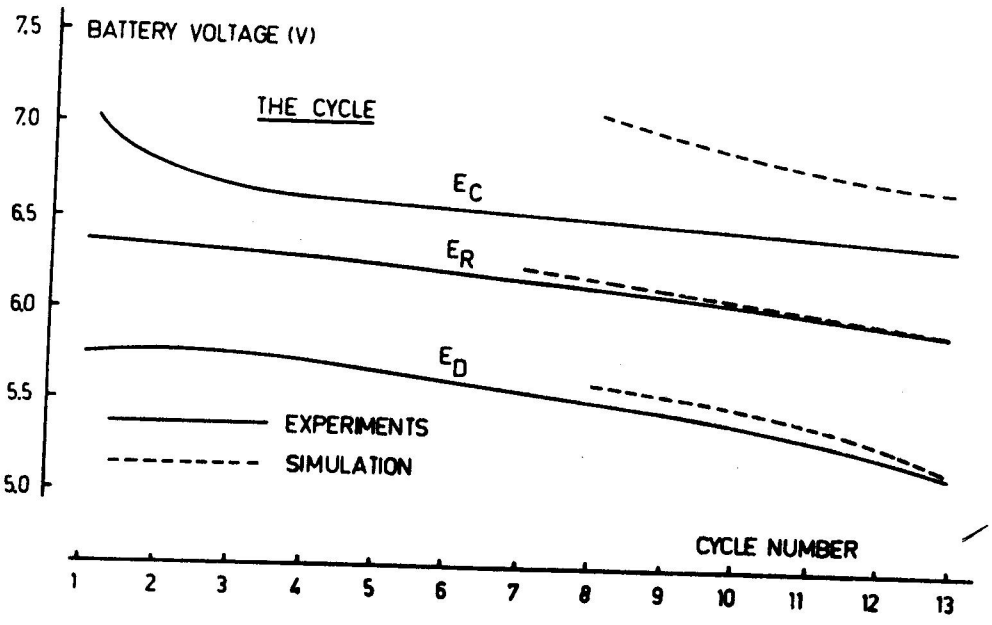

Fig. 10. Change in battery voltage at highest discharge current peak (E_D), at highest charge current peak (E_C) during 13 consecutive THE cycles and battery voltage at the end of each cycle (E_R).

5. CONCLUSIONS

The effect of state of charge of a battery upon the current voltage characteristics was described by a simple relation.
Calculation of the state of charge during duty cycle discharge was found to agree within 7% with experimental results and the actual battery voltage during electric vehicle operation agrees with the simulated performance.
With this model matching of power train and battery can be evaluated (9) and energy use and operation range can be predicted.

REFERENCES

1. K.E. White, Society of Automotive Engineers, paper 78216.
2. D. Simonsson, J. Appl. Electrochem. 3, 261 (1973).
3. W. Stein, Ph.D. Thesis, Aachen 1959.
4. K. Micka and I. Rousar, Collect. Czech. Chem. Commun. 40, 921 (1975).
5. J. Newman and W. Tiedeman, AI Ch.E.J. 21, 25 (1975).
6. C.M. Shephard, J. Electrochem. Soc. 112, 657 (1965).
7. W. Schleuter, ETZ Archiv. Bd 4, 91 (1982).
8. W. Visscher, W. de Zeeuw and R. van der Graaf, 5th International Electric Vehicle Symposium, Philadelphia 1978, paper 783107.
9. L.A.M. van Dongen, R. van der Graaf and W. Visscher, 6th International Electric Vehicle Symposium, Baltimore 1981, paper 8115.

THE EINDHOVEN EXPERIMENTAL ELECTRIC VEHICLE: VEHICLE DESIGN AND DRIVE TRAIN.

L.A.M. van Dongen, R. van der Graaf, Eindhoven University of Technology, Eindhoven, The Netherlands.

SUMMARY
At Eindhoven University of Technology a multidisciplinary team of chemical, electrical and mechanical engineers is collaborating on constuction of an electric commuter car/van.
A VW-Golf which concept appears to be very suitable for this purpose, has been electrified. Car-body and rear suspension were modified thus that a rapidly exchangeable battery pack could be placed in a central box.
Various ways of controlling the powerflow from the 16/33 kW Siemens dc-motor to the wheels will be tested in this vehicle.
Three systems, which are under construction, are described:

- battery switching, field weakening and a fixed ratio transmission
- battery switching, field weakening and automatic gear-shifting
- fully electronic control by means of choppers.

1. INTRODUCTION

During the last decade the importance of the development of electric road vehicles has widely been recognized. In the beginning much effort has been displayed in the construction of electrically driven buses and vans for a variety of reasons.
A group of interested persons at the Eindhoven University of Technology discerned the challenge which was put in this field by the passenger car as a replenishment of those activities. Especially in this application some features of the electric drive, such as battery weight, energy-efficiency of the drive line, selection and construction of components to be used, cost of these components, vehicle safety aspects, asked for a thorough investigation.
Optimization of a vehicle concept with respect to these features was considered necessary, and therefore a multi-disciplinary team was formed in which the chairs of Electrochemistry (Department of Chemical Engineering), Electromechanics (Department of Electrotechnical Engineering) and Transport Research (Department of Mechanical Engineering) are taking part.

On-the-road testing of various methods of motor control and types of battery would be an important part of the investigations.
It was expected that the project would give rise to a number of educationally very interesting studies for the final theses of postgraduate students, whereas the members of the multi-disciplinary working group hoped to learn a lot from each other. These expectations are largely being fulfilled.

2. VEHICLE CONCEPT

Specifications:
In an early stage the vehicle specifications of the Eindhoven Electric Vehicle (EEV) were set up:

- Top speed : 80 km/h
- Acceleration : 1.5 m/s^2 up to at least 50 km/h
- Operating range : 100 km
- Passenger capacity: 2 + 2 (two adults with two children or luggage)
- Rapidly exchangeable battery pack
- Distinct attention should be paid to the active (road-holding and vehicle handling characteristics) and passive safety (mechanical and electrical in the case of collision).

From these specifications the purpose of full compatibility of the EEV with normal urban and suburban traffic can be noticed. It will also be clear that the operational demands of this electric passenger car are strongly determined by the availability of electrochemical batteries. In fact the lead-acid battery still appears to be the only short term alternative for the independently moving road vehicle.

The restricted energy and power density and the excessive weight of this energy storage system are responsible for the limited speed, acceleration and operating range. For purposes of range extension and improvement of the battery service ability it was decided to install a rapidly exchangeable battery pack in the vehicle.

Technical concept:
To obtain a reasonable range the battery weight will amount to about one third of the gross vehicle weight. The car will show proper steering characteristics if this large proportion of mass has a low centre of gravity with a good weight distribution over front and rear wheels and a moment of inertia that is as low as possible with respect to the vertical axis through the car's centre of gravity.
Hence it can be concluded that the batteries should be placed near the middle of the car.
Crash safety will also be favoured in this case, as the batteries and connectors are situated away from the outskirts of the vehicle.
These considerations, together with the required quick exchangeability of the battery pack, led to the concept of a central battery case in the floor of the car body.
By integrating this case in the body a kind of backbone is created resulting in good structural strength and stiffness of the total construction.
This concept of a central battery case also facilitates meeting the already early discerned need for conditioning of the batteries [1].
This conditioning comprises:
- ventilating the battery compartment to remove the escaped hydrogen gas
- heating the batteries during winter time; in order to prevent dropping of the capacity to too low a level, the temperature should be kept above 15 ^{o}C
- cooling the batteries when the temperature would reach too high a level; above about 50 ^{o}C the active mass can deteriorate.

Selection and modification of a car:
After some preliminary design studies [2] it was decided to start from an existing passenger car or light van which would be modified in order to meet the requirements mentioned before. Thus a great deal of body engineering is avoided and the development efforts can be concentrated on propulsion systems and chassis modification on behalf of the battery pack.
In selecting a car the following criteria were applied:
- the car must have front wheel drive so that the voluminous battery case can readily be accomodated
- the rear wheel suspension should permit accomodating this case without drastic modification of this suspension
- the car should be able to carry the extra battery weight of some 5000 N with only minor changes; this implies that the gross vehicle weight will be at least 15000 N.
- sufficient room should be available between the front doors to accomodate the battery case and two seats
- the motor compartment should be able to house the different types of drive systems (see 3) that are to be tested.

It appeared that out of the small European cars the Volkswagen Golf fulfilled these requirements in the best way. Thus the EEV is built upon this type.
With type and weight of the vehicle known, the power requirements of the drive train can be stated. To maintain the fully loaded vehicle at its required top speed of 80 km/h, the propulsion motor should have a continuous power output of at least 13 kW.
Among the available electric motors the Siemens 1GV1, being a separately excited motor, especially developed for electric vehicles, fitted best into the specifications with:

- nominal power	17 kW
- maximum power	34 kW
- nominal speed	2200 rpm
- maximum speed	6700 rpm
- nominal voltage	130 V

With this motor the estimated acceleration of 1.5 m/s^2 can only de maintained until approximately 43 km/h; at higher velocities this value will gradually fall down.

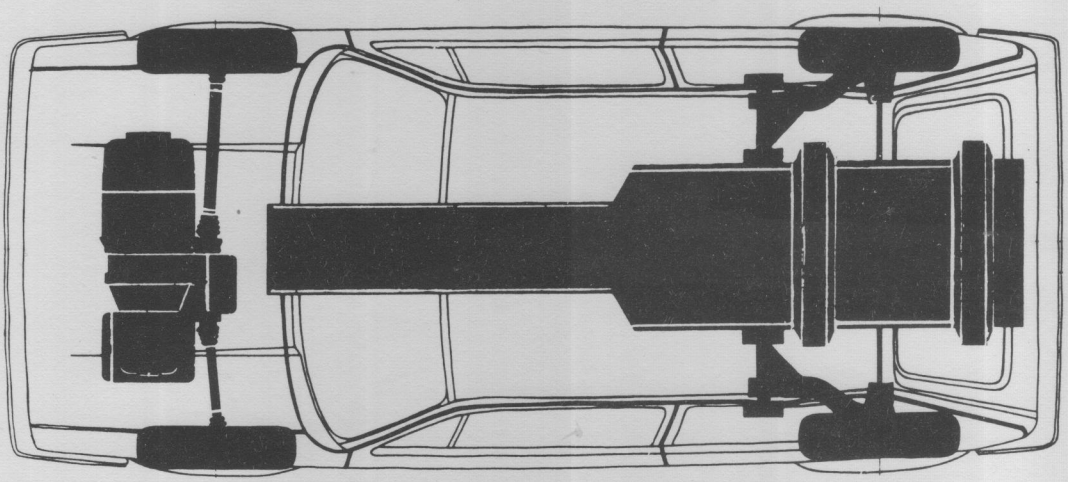

Fig. 1 Top view of modified car

In Figure 1 the top view of the changed car shows clearly the drive train, central battery case and modified rear axle.
According to the aim of testing various types of battery, the case has been constructed in such a way that batteries with different dimensions can be accomodated. The batteries are placed in a wheeled sledge which can roll in the case and which is provided with sliding contacts at its front side.

The specifications of the first battery pack to be used, are:

type	:	Varta 240-15, EV battery
voltage	:	20 x 6 V
capacity	:	180 Ah at 5 h discharge

Fig. 2

Interior of the modified Golf, showing the battery case construction

Maintenance of the original rear wheel suspension, trailing arms with an integral transversal anti-roll bar, would result in too high a battery pack location. This construction has therefore been replaced by totally independent wheel suspension with newly constructed inner supports for the trailing arms.

3.DRIVE SYSTEM AND MOTOR CONTROLLER

General description:

Many passenger car manufacturers are developing and testing several drive systems in various electric vehicles. Due to different vehicle characteristics and testing conditions it is almost impossible to obtain a reliable comparison of these drive trains. Moreover, the near-term objective arises of optimizing drive systems using currently available components with respect to operating range and primary energy consumption. For these reasons in the Eindhoven Electric Vehicle various drive systems are being constructed and tested under identical conditions.

The dc-series motor has long been regarded as an excellent choice for traction application because of its capability to deliver a large torque at low speeds. Control of the torque generated by the motor can be achieved by varying the magnitude of the supply voltage. A separately excited dc-motor, which provides the best combination of efficiency, performance and controlability for the near-term electric vehicle, is significantly different and has been chosen for the EEV. The speed of this motor can be controlled by field weakening in the speed range above nominal speed and by varying the armature voltage or circuit resistance in the speed range below nominal speed.
As a rule the motor is coupled to the propeller shaft by means of a step-down gear and the motor must therefore be capable of being adjusted over the entire speed range. Simulation studies, however, [3] demonstrate that from an energetical point of view a propulsion train using a variable transmission ratio has to be preferred to a drive system with a fixed gear ratio.

In general, three areas of control can be discerned over the motor speed range:

1. field weakening in the upper part of the range.
   As the field requires relatively low currents (up to 7 Amps approximately), field controllers are almost exclusively of the cheap single quadrant transistor-type.

   As only a limited control range is realized by field weakening, further adjustment is necessary:
2. adjustment of motor speed can be performed in various ways:
   - Continuously Variable Transmission
   - Automatic gearbox
   - Manually shifted gearbox
   - Hydrostatic transmission

   } motor control only by field weakening

   - Battery voltage switching
   - Armature current chopper (transistor or thyristor)

   The fourth and sixth type permit adjustment from zero vehicle speed. The other types necessarily need:
3. slipping devices for starting from standstill
   This function can be fulfilled by:
   - resistive motor control
   - friction type of coupling
   - hydraulic coupling
   - torque converter

In a preliminary study the control devices mentioned under points 2 and 3 have been reviewed and compared. The various possibilities have to be judged from different points of view, each of them delivering a number of criteria:

point of view	criteria
economical	cost energy efficiency

operational	reliability maintenance duration of life
vehicle handling	ease of operating smoothness
design	feasibility of optimal control feasibility of recuperative braking weight, dimensions, divisibility } of devices
environmental	noise

From these considerations it appeared to be desirable to construct and test three drive/control systems in the vehicle:
- voltage switching, field weakening and a fixed ratio transmission
- voltage switching, field weakening and automatic gear shifting
- fully electronic control by means of choppers.

In the first and second system also resistive control has to be comprised for low speeds.
In the following part the selected control systems will be described in more detail.

Resistive motor control

In the past this control was the most popular type in use because of its low cost and quiet and smooth operation. At high vehicle speeds the field chopper is responsible for motor control and at low speeds resistors are switched into the armature circuit, as shown in Figure 3. In order to provide a smooth operation a sufficient number of resistance steps is required. In the resistors, however, energy destined for propulsion is lost, and regenerative braking is impossible over this motor speed range. This greatly reduces the operating range in the typical type of driving of an electric vehicle: start and stop urban travel. The total amount of energy,which is lost in the resistors, can in fact be reduced by using a multi-speed gearbox, which allows the resistors to be switched out of circuit over a larger vehicle speed range. Because of the considerable energy losses in the resistors, purely resistive control does not deserve consideration for a modern electric vehicle.

Voltage switching

Another apparently simple form of speed control for an electric vehicle consists of a group of electric contacts in combination with some resistance elements. The battery pack is provided with several taps, at various voltages and the contacts reconnect the motor armature to various parallel and series combinations in order to give the appropriate motor voltage depending on desired speed. It is difficult to realize more than three or four acceleration steps, because the number of switching elements almost doubles with each step. Moreover, practical mechanical controllers are often extremely complex due to circuit demands, that are important for reasons of safety, and additional switching devices installed to ensure that all batteries are discharged uniformly.

An automatic voltage switching system has been designed, so that 30, 60 or 120 Volt is obtained at the motor terminals [4] . Figure 4 shows that the speed range ratio, that can be controlled by field weakening as stated above, has been quadrupled by simply changing the batteries from series to parallel connections. Only additional measures are required for bridging the start-up range.
Although the system just described does provide control of speed, a complete covering of the tractive effort/speed range cannot be realized. Moreover, the tractive effort falls off, because voltage switching occurs at no-load conditions in order to prevent arcing of the switches.
In order to limit the armature current at low vehicle speeds a resistor can be used. This can also be realized in a simple way by using a hydrodynamic torque converter. Although the damping charateristics of a torque converter are attractive, it has tremendous energetical disadvantages [5] :

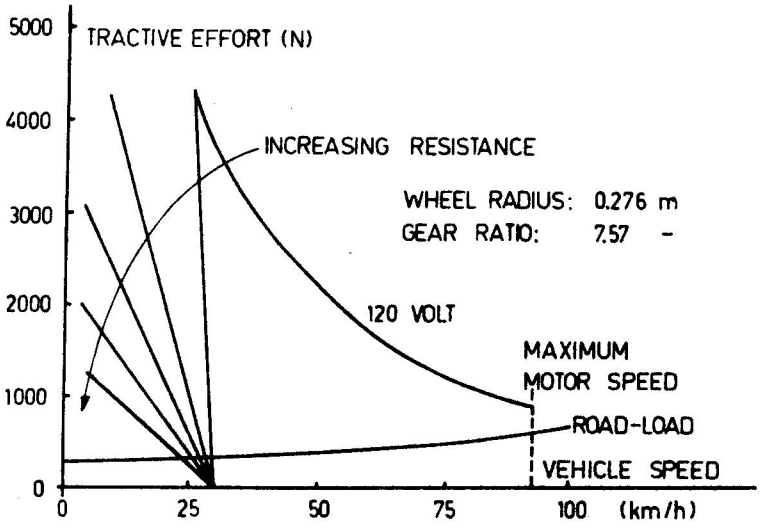

Fig. 3 Resistive motor control

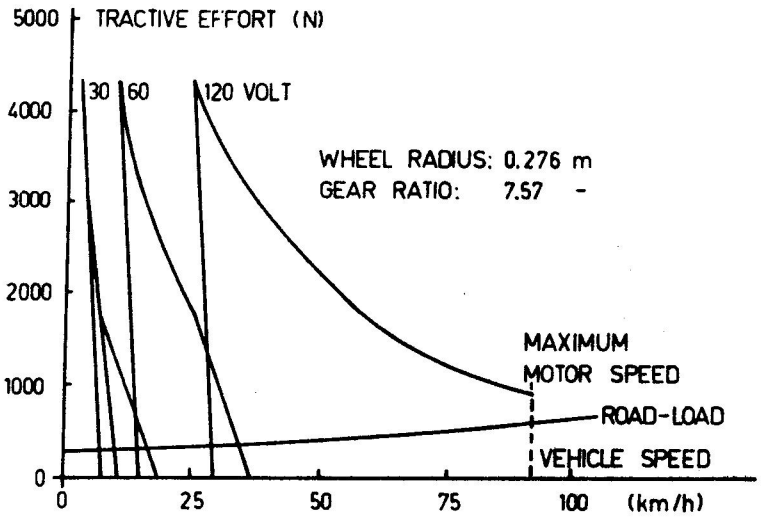

Fig. 4 Voltage switching

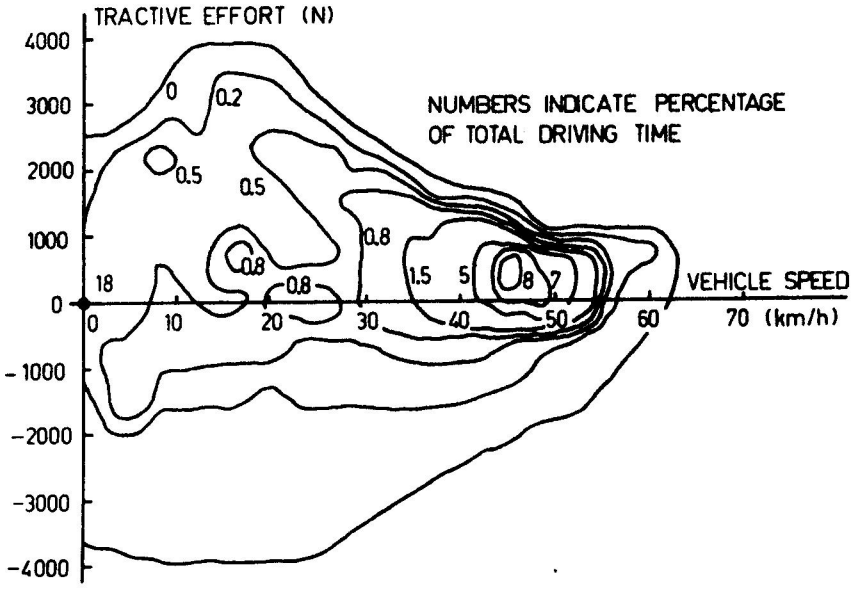

Fig. 5 Vehicle operation points

- torque converters have high losses in the converting range and a minimum slip of at least 2% occurs in the coupling range
- a torque converter requires an oil pump, the losses of which are high and proportional to the rotational speed.

For this reason a drive train having a fixed gear ratio of 7.57 and the dc motor controlled by a voltage switching system with a starting resistor is being tested in the vehicle now.
By mounting a multi-speed gearbox the number of unattainable operating points in the tractive effort-speed plane can considerably be reduced. The transmission ratios have to be matched in order that:

- as many as possible operating points can be adjusted
- an as high as possible average motor efficiency is realized
- gear changes and frequent speed variations in town traffic do not coincide.

In order to have an impression of the vehicle operating conditions in town traffic several driving cycles have been recorded in typical Dutch cities as The Hague and Delft. After analysis of these recordings and conversion of the results, curves of constant operating time have been constructed in the force-speed plane of the electric vehicle, as is indicated in Figure 5 [6] .
For convenience of handling during city driving a standard automatic gearbox has been modified. In order to minimize the power losses in the gearbox, the torque converter has been replaced by a primary gear wheel reduction and the oil pump power has been optimized by using a separate constant speed oil pump instead of the standard oil pump. Figure 6 shows that the gear ratio of the primary reduction has been selected in such a way that gear changes only occur at less frequent operating points. The individual overall gear ratios stand at 16.58 , 9.41 and 6.50 for the first, second and third gear respectively. Since the motor operates at speeds between 2200 abd 5500 rpm and the resistor is only switched in when the vehicle accelerates from standstill, high efficiency and sufficient operating range can be attained by this approach.
Due to motor synchronization during shifting procedures the operational comfort of the drive system is expected to be at least comparable with that of vehicles with an internal combustion engine and an automatic gearbox.

Fully electronic motor control

Another possible approach is to use an electronic switch in the armature circuit. The switching element is turned on and off at a certain frequency and thus has the effect of chopping the battery voltage.
In this way the armature voltage can be varied smoothly from 0 Volt to the full battery voltage by controlling the time intervals during which the switch is open. The chopper may roughly be regarded as a dc transformer. Since the losses in the chopper stand at about 4% of the power transmitted, the motor power nearly equals the power supplied by the battery. Without much extra expense these choppers allow regenerative braking in the entire speed range.
In principle it is possible to dispense with a multi-speed gearbox when a drive system with a dc motor and a dc chopper is used on the condition that the motor has been designed to handle the high currents drawn during the starting phase (Figure 7). Due to the infinitely variable adjustment of the propulsion power a smooth speed control is realized. When the vehicle is moving at low speeds the field current stands at its maximum and speed is adjusted by varying the armature voltage with the chopper. At vehicle speeds requiring motor speeds higher than its nominal speed, the armature chopper applies full battery voltage to the motor terminals and the vehicle speed can be controlled by variation of the field current.
Yet the use of a multi-speed gearbox has the following advantages (Figure 8):

- during the starting phase a higher gear ratio can be engaged, which reduces the initial current drawn from the battery
- with the possibility of selecting different gear ratios it is easier to meet demands for hill climbing
- since separately excited dc motors are less efficient at low rotational speeds, variable gear ratios allow highly efficient motor operation.

A thyristor chopper for the armature circuit is being developed which will control the Siemens motor coupled to either the step-down gear or the automatic gearbox.

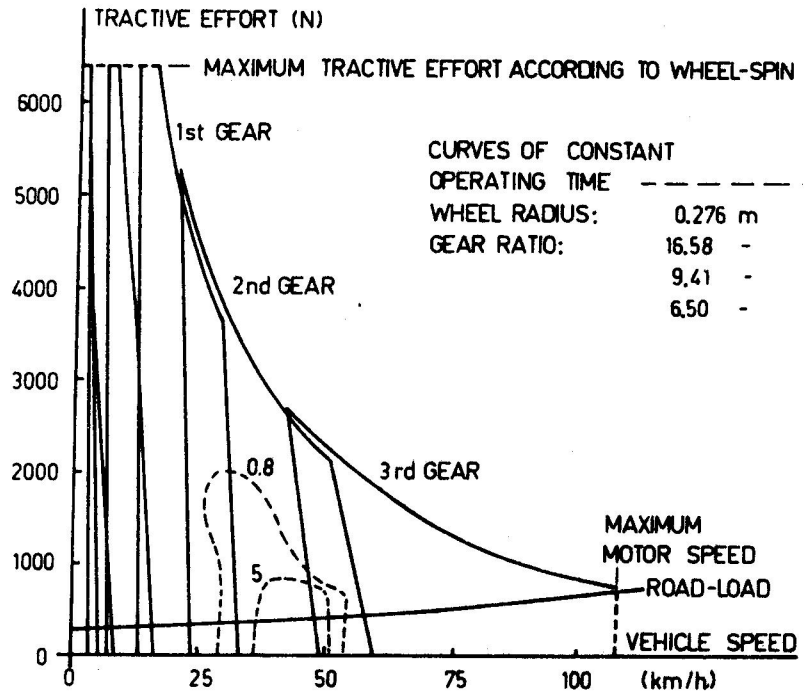

Fig. 6 Voltage switching and a multi-speed gearbox

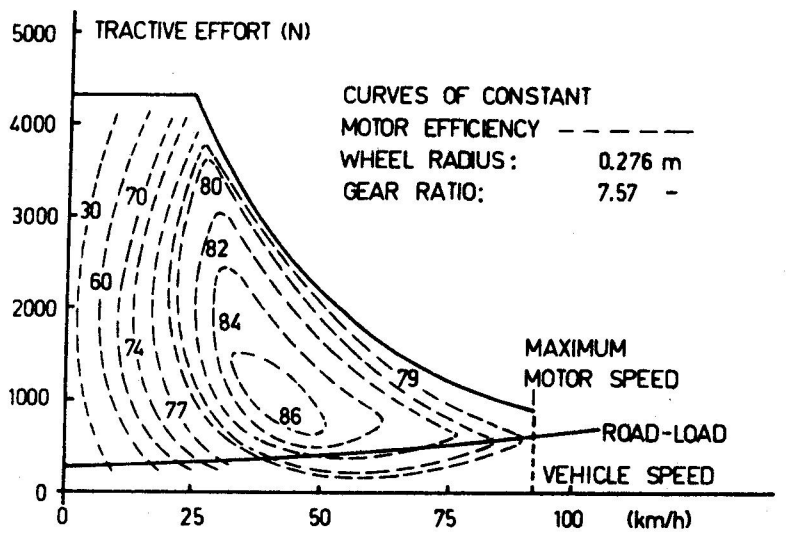

Fig. 7 Fully electronic motor control

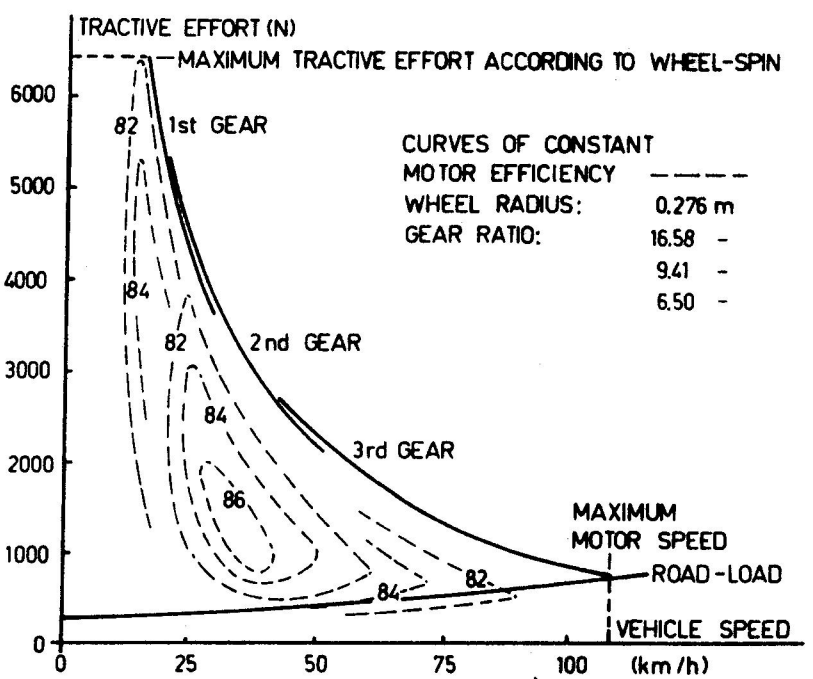

Fig. 8 Fully electronic motor control and a multi-speed gearbox

The efficiency of these approaches appears to be high, since the losses in the motor controller are small and regenerative braking is possible. Other advantages are operational comfort and acceptable range. A disadvantage of these drive systems is the costly armature controller, which must be able to handle currents up to the 350 Ampere.

References

1. W.H.M. Visscher, W. de Zeeuw, R. van der Graaf: Experiments on Lead-Acid Batteries of an Electric Vehicle.
   EVS-5 Philadelphia, Oct. 1978.
2. W.A. Koumans: The Electric Car Project of the Eindhoven University of Technology.
   PPL Conference Publication, no. 14.
3. L.A.M. van Dongen, R. van der Graaf, W.H.M. Visscher: Theoretical Prediction of Electric Vehicle Energy Consumption and Battery State-of-Charge during Arbitrary Driving Cycles.
   EVC Symposium VI, Baltimore, Oct. 1981.
4. H.C.J. Zeegers: Torque control of a shunt wound dc-motor of an electric vehicle by means of continuous field control and stepwise adjustment of the armature voltage.
   Drive Electric Amsterdam '82. Oct. 1982.
5. Leo A.M. van Dongen: Efficiency Characteristics of Manual and Automatic Passenger Car Transaxles.
   Society of Automotive Engineers, paper 820741.
   Troy, Michigan, June 1982.
6. S.W.M. van Vuuren: Analyse van een stadsrit. Eindhoven University of Technology, Dept. of Mech. Eng. Internal report.

TORQUE CONTROL OF A SHUNT WOUND DC MOTOR OF AN ELECTRICAL VEHICLE BY MEANS OF CONTINUOUS FIELD CONTROL AND STEPWISE ADJUSTMENT OF THE ARMATURE VOLTAGE.

H.C.J. Zeegers, Eindhoven University of Technology, Eindhoven, The Netherlands.

ABSTRACT

It is shown that notching armature voltage and continuous field control can be a compromise solution for EV-drives. For the given vehicle parameters the necessarily series resistors are determined. An analysis of field control at different armature voltages is given for both stationary and dynamic conditions. Flow chart and block diagram of the control system are given. Attention is paid to the MOSFET-implemented field controllers and to the measurement of the electromagnetic torque using armature and field current.

1. Introduction

In the early seventies a group at the university of Eindhoven started to work on the subject of electrically driven vehicles in order to provide authorities with reliable data in this field. In 1973 it was decided to develop an electric passenger car.

1.1. The EV of the Eindhoven University of Technology

The vehicle should meet the following requirements [7]:

1. capacity : 2 adults + 2 children (so called 2+2 car);
2. range : 100 km;
3. topspeed : approx. 90 km/h;
4. cruising speed : 50-70 km/h;
5. acceleration : 1.5 m/s^2 up till 50 km/h;
6. gradients : 20% at stall condition;
7. rapidly exchangeable battery pack;
8. active safety (good road-holding, handling and suspension);
9. good passive safety considering the presence of the battery pack;
10. the electric drive should be such that it offers high efficiency and makes the car easy and pleasant to drive, also for persons used to cars with internal combustion engine. Besides that it should be cheap and servicing should be easy to be carried out by garage personnel with little extra training.
11. regenerative breaking.

After research by the groups transport research [3], [4] and electrochemistry [4], [10], it was decided to modify a VW-Rabbit car and e-

quip it with a 120 V - 240 Ah lead-acid battery. The battery pack is made up of twenty 6 V-batteries. This concept resulted in a total vehicle weight of approximately 1500 kg.

Taking into consideration the requirements for the electrical drive (see point 10), it was concluded that while an armature-chopper has the advantage of easy control and good efficiency, it has the disadvantage of being expensive and containing a lot of advanced electronics. It was expected that stepwise armature voltage adjustment with field control in addition would offer a good compromise solution. In order to verify this statement both systems should be investigated.

The following program was started:

A. Development of a system based upon stepwise armature voltage adjustment by means of electromagnetic switches and continuous field control by a transistor chopper. At very low speeds additional armature resistors are required.

B. Development of a system with an armature and field current chopper.

C. Comparison of A. and B.

This paper deals with part A. of the project. To realize A. a fixed reduction between machine shaft and wheels of 7.6 had to be considered, which means that the machine speed must be controlled over a large range. Driving backwards is possible by reversing the field current. In order to realize regenerative breaking, with this circuit configuration it is best to use a DC-machine with separate excitation.

A Siemens-machine, type 1GV1 appeared to be the most suitable traction machine commercially available. Nominal and maximum values are specified in table 1 [9].

Mechanical and electrical performances are shown in fig. 1.a,b.

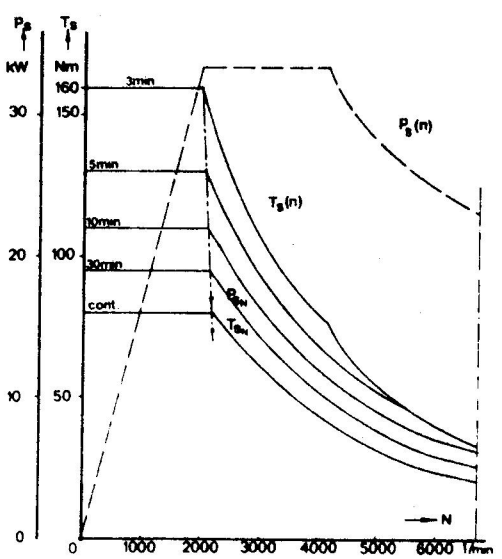

Fig. 1.a. The mechanical performances of the 1GV1.

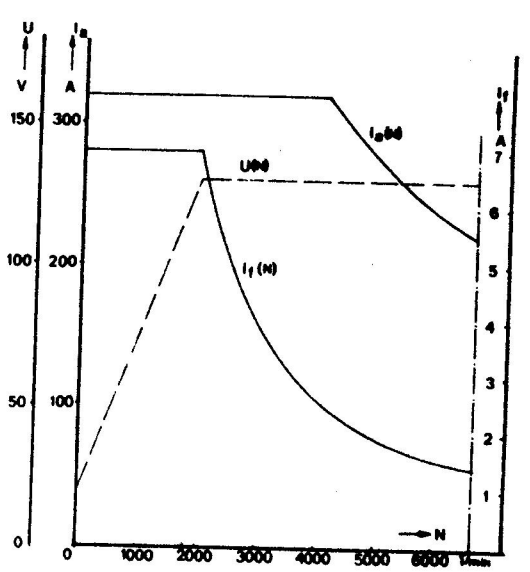

Fig. 1.b. The electrical performances of the 1GV1.

	Nominal	Maximum
Armature voltage	130 V (at nom.motor cond.)	180 V
Armature current	150 A	320 A (3 min.)
Excitation voltage	100 V	-
Excitation current	7 A	-
Speed	2200 min^{-1}	6700 min^{-1}
Torque	75 Nm	160 Nm
Power	17 kW	33.5 kW

Table 1.

1.2. Speed control of the separately excited DC-machine

A seperately excited DC-machine offers two gates, named armature and field winding terminals, through which it can be controlled. Figure 2 shows a machine connected to a voltage source U and loaded with a torque T_L plus friction torque T_{fr}.
The total inertia of armature plus load is called J.

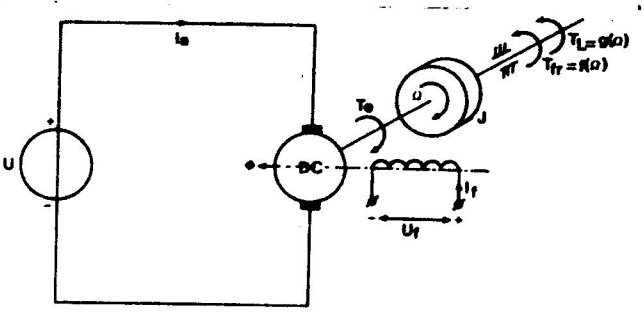

Fig. 2. Electrical drive with a DC-machine.

This drive can be described by the following equations:

$$U = I_a R_a + L_a \frac{dI_a}{d\tau} + E + \frac{I_a}{|I_a|} U_b \qquad (1)$$

$$E = c_m \Omega \Phi_a \qquad (2)$$

$$T_e = c_m I_a \Phi_a \qquad (3)$$

$$T_e = T_L + T_{fr} + J \frac{d\Omega}{d\tau} \qquad (4)$$

$$U_f = \frac{d\Phi_s}{d\tau} + I_f R_f \qquad (5)$$

Due to leakage, Φ_s and Φ_a differ slightly.
If we consider the system under quasi-stationary conditions ($\frac{dI_a}{d\tau} \approx 0$, $\frac{d\Omega}{d\tau}$ is small) and if we neglect the armature reaction and the voltage drop U_b across the brushes, which is mostly 1 - 1.5 V, the equation of motion can be derived from (1), (2) and (3). This gives the relationship between electromagnetic torque T_e and angular speed Ω.

$$T_e = \frac{c_m \Phi_a}{R_a} (U - c_m \Omega \Phi_a) \qquad (6)$$

A general relation is found when the parameters are made dimensionless. Relating the magnitudes to their nominal values [6] we get:

$$t_e = \frac{T_e}{T_{e_N}} = \frac{T_e}{c_m \Phi_{a_N} I_{a_N}} \tag{7}$$

$$\omega = \frac{\Omega}{\Omega_N} \tag{8}$$

$$u = \frac{U}{U_N} = \frac{U}{c_m \Phi_{a_N} \Omega_N} \tag{9}$$

$$\varphi = \frac{\Phi_a}{\Phi_{a_N}} \tag{10}$$

$$r = \frac{R_a}{R_N} = \frac{R_a}{U_N / I_{a_N}} \tag{11}$$

One must be aware of the fact that U_N is defined as armature voltage under no-load conditions at nominal speed and nominal excitation. This value differs from the one given by the manufacturers for nominal motor conditions. The magnitude $R_N = \frac{U_N}{I_{a_N}}$ is a fictive value which proves to be convenient once introduced. By using (6) up to (11) the general equation of motion is obtained.

$$t_e = \frac{u\varphi}{r} - \frac{\varphi^2 \omega}{r} \tag{12}$$

Formula (12) includes three principles of affecting the torque speed curve, namely by u, φ and r. The specific influence of each of them is shown in fig. 3a, b and c.

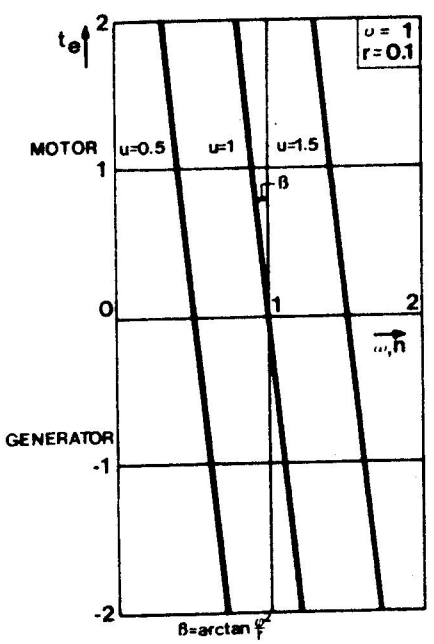

Fig. 3a. Armature voltage control.

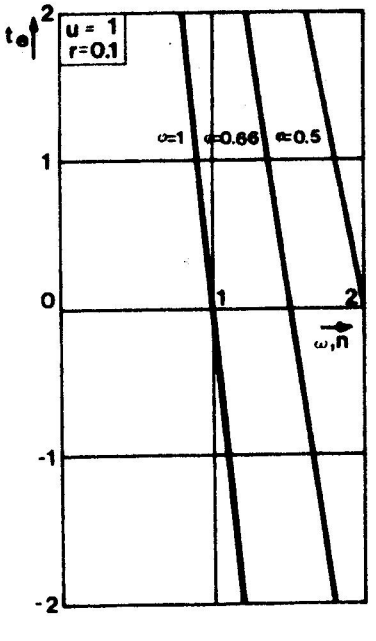

Fig. 3b. Field control.

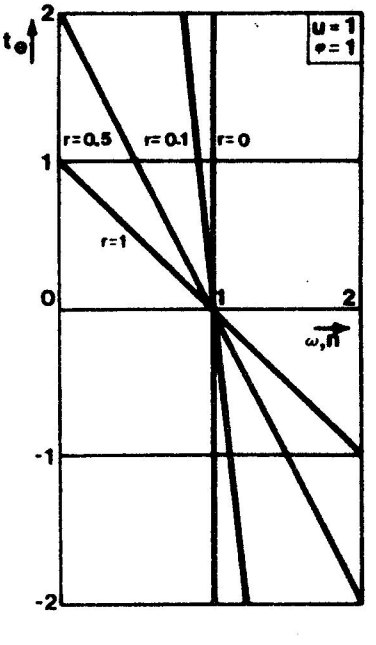

Fig. 3c. Resistive control.

The value r = 0,1 appears to be a quite common practice.

ad a. Speed control by armature voltage control is a very good method because of the high efficiency and the maximum torque being available at any speed. The speed range is determined by the machine parameters.

ad b. Speed control by field control offers fairly good efficiency and constant output power up to high speeds, however, from very high speeds (approx. 2 x Ω_N) the power is mostly limited due to commutation considerations.

Compared to method a, field control used at voltages smaller than u = 1 will give a lower machine efficiency, because of the higher losses due to higher armature current. Besides that, the maximum power which can be converted is smaller. However, the losses in the armature controller itself are larger in a chopper than in a stepwise controller, which must be used in combination with field control, due to the fact that in the latter losses only are caused by the necessarily excitation power for electromagnetic switches.

Moreover, these losses can be reduced by applying transistor choppers, such that the excitation current is limited after switching on.

ad c. Resistive speed control causes substantial energy dissipation especially at high armature current. Therefore it has a low efficiency and must be limited to the minimum.

2. Speed control by means of stepwise voltage adjustment and continuous field control

In the here considered drive the battery pack is devided in four blocks of 30 V each by a number of electromagnetic switches. By connecting these blocks in series and/or parallel, armature voltages of 30 V, 60 V and 120 V are obtained through which the machine speed is regulated in coarse steps. The speed can be regulated finely at each armature voltage by electronic control of the field. As the field windings are also fed from the battery pack, they had to be split in two parts in order to obtain nominal excitation current at each armature voltage.

Area	Switches in on-state								
	S1	S2	S3	S4	S5	S6	S7	S8	HS
30 V + R_V + R_p				X		X		X	X
30 V + R_V		X		X		X		X	X
30 V	X	X		X		X		X	X
60 V	X	X	X		X			X	X
120 V	X	X	X				X		X

Table 2.

R_v and R_p are incorporated for current limiting at low speed. Table 2 shows which switches have to be closed in a certain situation; switches which absolutely may not be closed at the same time cancel each other by normally closed interlocks.

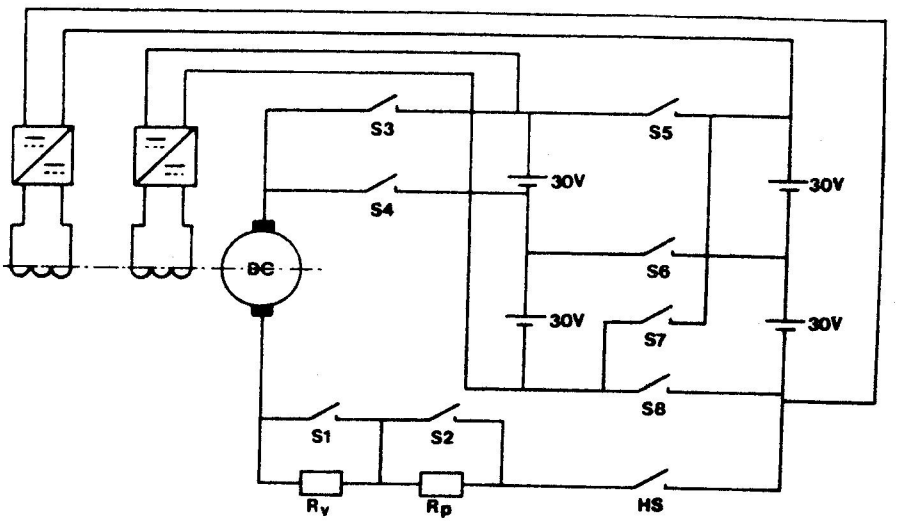

Fig. 4. Armature and field winding circuits.

2.1 Characteristics

The speed-torque curves for the above mentioned conditions are obtained by using (12) and the specific nominal values of the 1GV1-machine. These values are partly supplied by the manufacturer and partly determined by measurements.

$$T_{e_N} = 80 \text{ [Nm]}; \quad T_{S_N} = 75 \text{ [Nm]}$$

$$U_N = 124 \text{ [V]}$$

$$c_m \Phi_{a_N} = 0.54 \text{ [Wb]}$$

$$R_{a_N} = 0.83 \text{ [}\Omega\text{]}$$

$$N_{s_N} = 2200 \text{ [min}^{-1}\text{]}$$

$$R_a = 60 \cdot 10^{-3} \text{ [}\Omega\text{]}; \quad r = 0.07$$

While calculating T_{e_N} no attention has been paid to the reduction of the magnetic flux Φ_a due to armature reaction and not-ideal commutation. For these reasons the effective flux will be smaller than the flux produced by the field windings only and used to derive (12). Furthermore the torque at the machine shaft (T_S) will be smaller than T_e when the machine operates as a motor and larger when the machine operates as a generator due to iron and friction losses which depend upon speed and excitation. However, in the following we assume T_S to be linear with T_e. Furthermore nominal battery voltages are used in the characteristics and internal battery resistance is neglected.

Fig. 5 shows machine shaft torque versus machine speed and tractive effort versus car speed for armature voltages of 30 V (u = 0.24), 60 V (0.48) and 120 V (0.96) at different flux values.

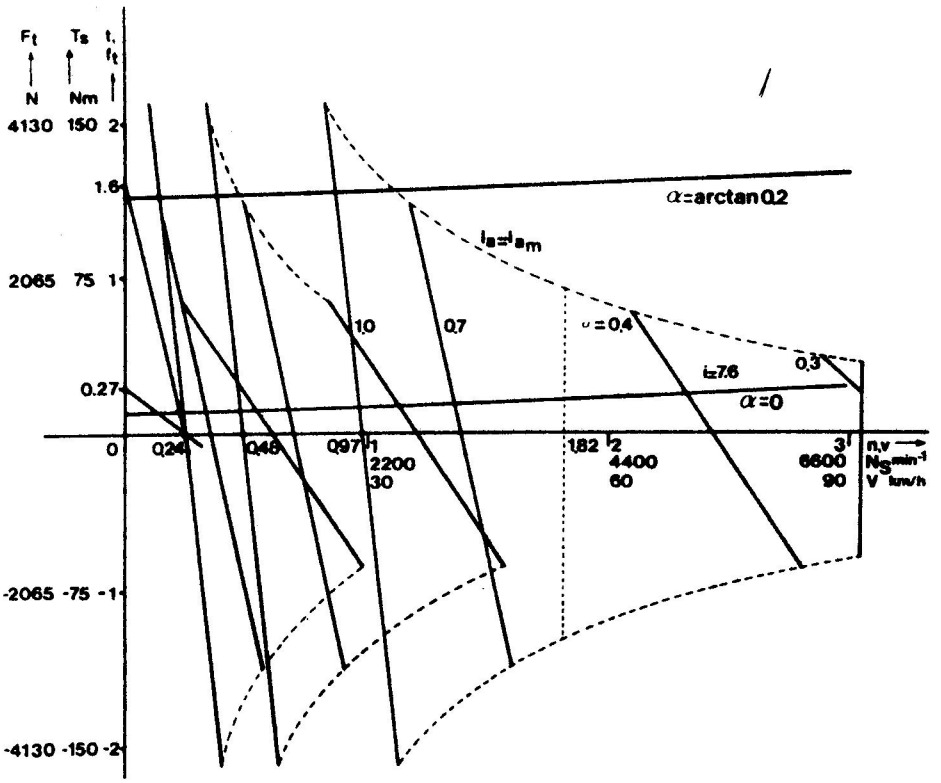

Fig. 5. Static machine characteristics and load characteristics for i = 7.6 with α = 0 and α = arctan 0.2.

Tractive effort and car speed are determined by the mechanical reduction and the wheel radius according to:

$$F_t = T_s \frac{i}{r_w} \tag{13}$$

$$V = \frac{2\pi}{60} \cdot N_s \cdot \frac{r_w}{i} \tag{14}$$

The torque is limited at all voltages by the maximum permissible armature current I_{a_M} which is constant up to $N_S = 4000\ \text{min}^{-1}$ ($n_S = 1.82$) and thereafter speed dependent due to the machines commutation. This dependence can be approximated by a linear function of n_S. The following equations for t_M are found.

As $|t_M| = |i_{aM}|\varphi$ we get:

$$|t_M| = 2.13\,\varphi \qquad n < 1.82 \tag{15}$$

and

$$|t_M| = (3.18 - 0.58n)\varphi \qquad 1.82 < n < 3.05 \tag{16}$$

The stationary load characteristics can be calculated with the well-known formula [2]:

$$T_S = \left(\frac{1}{2}\rho\left(\frac{2\pi}{60}\frac{r_w}{i}N_s\right)^2 A_F c_w + mg(f\cos\alpha + \sin\alpha)\right)\frac{r_w}{i} \qquad (17)$$

The characteristics for $\alpha = 0$ and $\alpha = \arctan 0.2$ are drawn in fig. 5.

2.2. Extra series resistors at low speeds

In order to limit the armature current at standstill and at very low speeds to a value just high enough to produce at maximum field excitation the desired load torques, series resistors are incorporated. Two cases can be distinguished, namely:

a. Driving during a short time with a maximum torque of 120 Nm ($t = 1.6$), for instance in parking garages and on slopes.
b. Driving during a long time with approx. 11 Nm (say 20 Nm; $t = 0.27$) while looking for a parking place or while driving in a trafic line.

The required relative resistances at standstill ($\omega = 0$) with maximum field ($\varphi = 1$) can be calculated using (12).
By taking into account the armature resistance $R_a = 0.06$ [Ω] the following values for R_v and R_p are found:

$R_v = 0.065$ [Ω]
$R_p = 0.615$ [Ω]

The machine characteristics for these resistances are also shown in fig. 5. Both resistances are switched off at a machine speed of 440 min^{-1} (car speed of 6 km/h), moreover R_p is switched off when the accelerator is pushed in more then 20% ($p > 0.2$).
The switching diagram is shown in fig. 8.

2.3. Analysis of field control at stepwise armature voltage adjustment

In order to design a control system which is based upon field control it is essential to know certain parameters such as the transfer function $(\frac{d\,te}{d\,\varphi})$ and the position of the maximum EM-torque in the φ-n plane at different armature voltages.

2.3.1. Quasi-stationary conditions

For these conditions $t_e = f(\varphi)$ is analysed:

$$t_e = \frac{\varphi}{r}(u - \varphi\omega)$$

1. The zeros are found at $\varphi = 0$ and $\varphi = \frac{u}{\omega}$.
2. The maximum EM-torque will be produced when the total voltage drop across the armature circuit resistances equals the back E.M.F.: $i_a r = \varphi\omega = \frac{u}{2}$. Its magnitude is: $t_{e_M} = \frac{u^2}{4\omega r}$.
3. The minimum EM-torque (maximum torque as generator) is limited by the maximum value of the field ($\varphi = 1$) and has a magnitude of: $t_{e_M} = \frac{1}{r}(u - \omega)$.

The EM-torque as a function of φ and e at constant armature voltage u is shown in fig. 6. Also shown is the static transfer curve $\frac{dt_e}{d\omega} = f(\varphi, e)$.

Fig. 6 shows that for small back E.M.F. (i.e. $e < \frac{u}{2}$), increase of the field will result in higher EM-torque and for high back E.M.F. (i.e. $e > \frac{u}{2}$) in lower EM-torque. The latter is almost always the case in motor applications of the DC-machine, however, not in the one considered here.
All points in the φ-ω plane, at which under motor conditions the EM-torque is maximum, lie on a orthogonal hyperbole which is determined by the armature voltage, i.e.

$$\varphi\omega = \frac{u}{2} = C$$

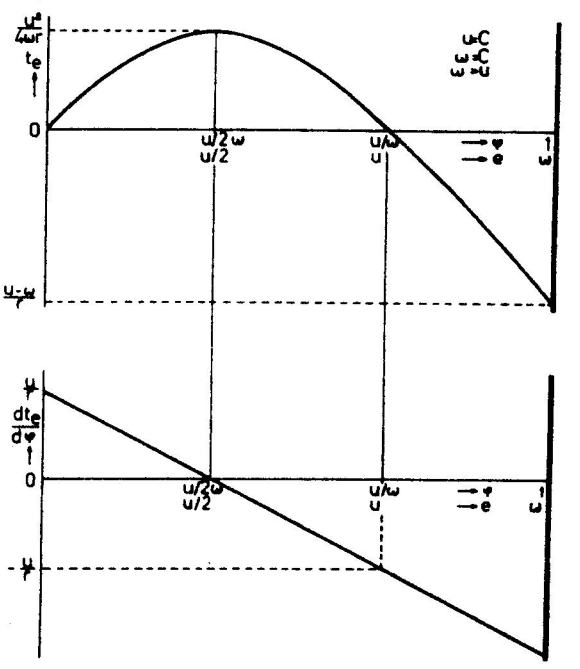

fig. 6.a EM-torque as a function of magnetic field at constant speed.
fig. 6.b Transfer curve $\frac{dt_e}{d\varphi} = f(\varphi)$ at constant speed.

The constant C for the armature voltages 30, 60 and 120 V is respectively: 0.12, 0.24 and 0.48.
Another important factor involved, is the magnitude of the armature current which must be held within certain limits. Curves for maximum permissible armature current under motor conditions as well as under generator conditions are also orthogonal hyperboles:

$$\varphi\omega = u - i_{a_M} \cdot r \qquad (19)$$

with $i_{a_M} = \pm 2.13$ for $\omega < 1.82$

and $i_{a_M} = \pm (3.18 - 0.58\,\omega)$ for $1.82 < \omega < 3.05$

All the curves mentioned and the one for armature current equal to zero are drawn in figure 7 for the distinct voltage levels and armature circuit conditions.
The criteria for changeover between armature voltage levels under motor conditions differ from those under generator conditions.

- Changeover under motor conditions ($T_s > 0$):
  As changeover must occur while the armature current is zero, the machine speed must be high enough to get a back E.M.F. equal to the next voltage level at maximum field ($\varphi = 1$).
  This means $\omega = u$. The following values are found: (20)

$$n_{30\to60} = 0.48; \quad N_{s30\to60} = 1056 \text{ min}^{-1}$$

$$n_{60\to120} = 0.96; \quad N_{s60\to120} = 2112 \text{ min}^{-1}$$

- Changeover under generator conditions ($T_s > 0$):
  In this case it is important to keep the breaking torque which can be produced as high as possible. This means that the maximum power delivered by the machine just after switching must be equal to the maximum power before switching, taking into account the field limit $\varphi = 1$ befor switching and the armature current limit $i_a = 2.13$ after.
  From this it follows that:

$$n = \frac{u_H}{2} + \sqrt{\left(\frac{u_H^2}{4} + i_{a_M} r\left(\frac{u_H}{2} + i_{a_M} r\right)\right)} \qquad (21)$$

Herein is u_H the highest of the two involved armature voltages at a certain switching point.

Hence $n_{120\to60} = 1.05; \quad N_{s120\to60} = 2310 \text{ min}^{-1}$

and $n_{60\to30} = 0.58; \quad N_{s60\to30} = 1276 \text{ min}^{-1}$

Figure 7 gives a complete survey of the requirements of the field control system, while figure 8 shows the exact situation of switching points at certain armature circuit conditions. The following conclusions with respect to this control system can be drawn for the distinct areas:

Area I : $U = 30$ V; $R \geq 0.125\ \Omega$; $-320 \text{ A} < I_a < 320$ A.
- The maximum permissible armature current cannot be exceeded.
- The transfer function $\frac{dt_e}{d\varphi}$ is possitive except for $260 < N_s < 440$, so that the field in this range is limited according to $\varphi = -2.27.10^{-3} N_s + 1.60$.

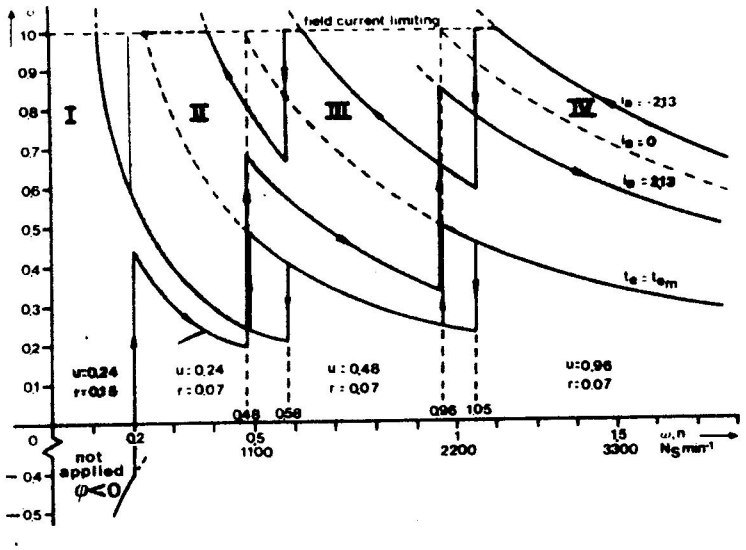

Fig. 7. Notching curves for maximum EM-torque and maximum current in the φω- plane.

Area II : U = 30 V; r = 0.06 Ω; $-320\ A < I_a < 320\ A$.

- The armature current must be limited in both positive and negative direction.
- In the largest part of the area the transfer function $\frac{dt_e}{d\varphi}$ is negative. During testing it appeared to be satisfactory to consider $\frac{dt_e}{d\varphi}$ negative all over the area.

Area III : U = 60 V; r = 0.06 Ω; $-320\ A < I_a < 320\ A$.

- The armature current must be limited in both directions.
- The transfer function $\frac{dt_e}{d\varphi}$ is negative all over the area.

Area IV : U = 120 V; R = 0.06 Ω; $-I_{a_M} < I_a < I_{a_M}$; $I_{a_M} = f(N)$; conditions: Identical to area III.

As the exact situation of the curves depend on the battery condition in such a way that under poor battery conditions the curve for maximum torque will possibly become higher situated in the φω-plane than the maximum motor current curve, it is necessary to take precautions in order to prevent the torque from falling to a very low value. Therefore the field in area II, III and IV is kept above the value of 0.2.

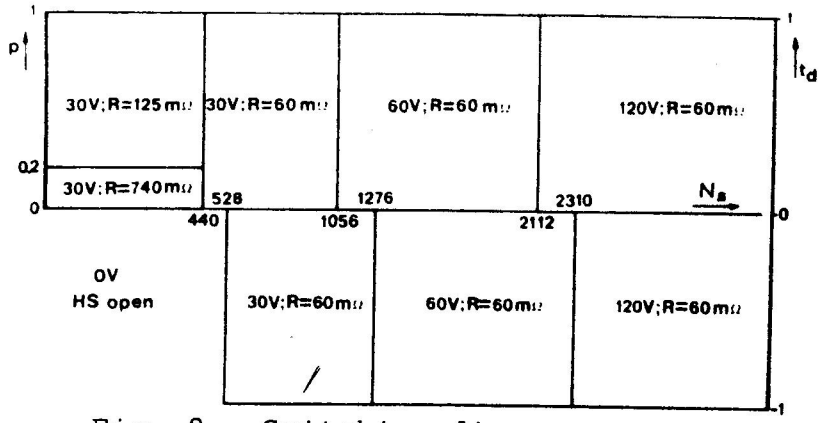

Fig. 8. Switching diagram.

2.3.2 The dynamic behaviour of the separately DC-machine with field control

In the preceding pages field control has been regarded under quasi-stationary conditions which means that changes occur so slowly that the system, the elctrical as well as the mechanical part, can follow immediately. The system behaviour under these circumstances is the most important for EV-applications, however, with respect to system design the dynamic behaviour is also most interesting [1], [5] and [8].

The transfer function $\frac{T_e}{\varphi}$ or $\frac{T_e}{U_f}$ can only be determined for small signals around a working point due to the non-linearity of machine equations and the load characteristic. The following transfer function can be derived in the Laplace-domain; assuming a linear relationship exists between Φ_s and Φ_a.

$$H(s) = L\left\{\frac{T_e}{U_f}\right\} = \frac{-2c_1\Omega_{a_o} c_m (E_o - I_{a_o} R_a)}{2c_1\Omega_{a_o} R_a + c_m^2 \Phi_o^2} \cdot$$

$$\frac{\left(1+ \frac{J}{2c_1\Omega_{a_o}} s\right)\left(1- \frac{I_{a_o} L_a}{E_o - R_a I_{a_o}} s\right)}{\left(\frac{JL_a}{2c_1\Omega_{a_o} R_a + c_m^2\Phi_o^2} s^2 + \frac{JR_a + 2c_1\Omega_{a_o} L_a}{2c_1\Omega_{a_o} R_a + c_m^2\Phi_o^2} s + 1\right)\left(\frac{R_f}{L_{f_o}} + s\right)} \qquad (22)$$

Where: $\Omega_o = \frac{i}{r_w} V_o$ $\qquad$ $c_1 = \frac{1}{2} \rho A_F c_w \frac{r_w^3}{i^3}$

$E_o = c_m \Phi_o \Omega_o$ $\qquad$ $J = \frac{r_w^2}{i^2} \lambda m$

λ is a constant necessary to bring into account the rotating parts of the drive. The parameters with subscript "0" refer to the chosen working point. With the wellknown techniques from control engineering it is possible to determine the response to a step input signal $U_{f\sim}$.
It appears that:

- the final value of the response has a sign <u>opposite</u> to that of $U_{f\sim}(E_o - I_{a_o}R_a)$, (see also fig. 6a.).
- the differential coefficient $\frac{dT_e}{d\tau}$ at time $\tau = 0$ has the <u>same</u> sign as that of the disturbance $U_{f\sim}$.

This means that when $E_o - I_{ao}R_a > 0$ the system at first shows an inverse response (see fig. 9). The transfer function has a zero in the right part of the complex s-plane and is called a *nonminimum phase-shift transfer function.* The physical explanation for this phenomenon is the existance of the electrical inertia of the armature, through which the transient at the beginning is determined by the field only.

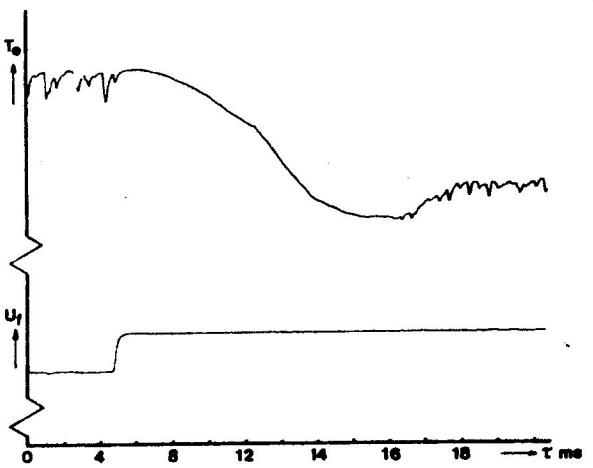

Fig. 9. Torque response to step input field winding voltage.

3. Realisation of the control system

In principle an armature current or field control is sufficient to control speed, acceleration and regenerative breaking. However, due to the speed dependence of the field, the accelerator or brake pedal position would need to be readjusted continually in order to keep the desired acceleration or deceleration. By applying an extra torque control loop, the driving or breaking torque is kept constant as far as the armature or field current limits are not exceeded.
In the area where the series resistors are incorporated in the armature circuit and hence $\frac{dt_e}{d\varphi} > 0$, the field is controlled straightaway by the accelerator pedal signal. Fig. 10a, and b shows the block diagrams of the distinct control systems.

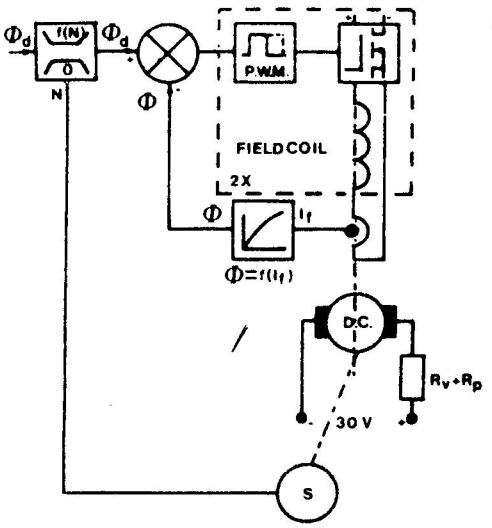

Fig. 10a. Field control in the area U=30 V; R≥125 mΩ

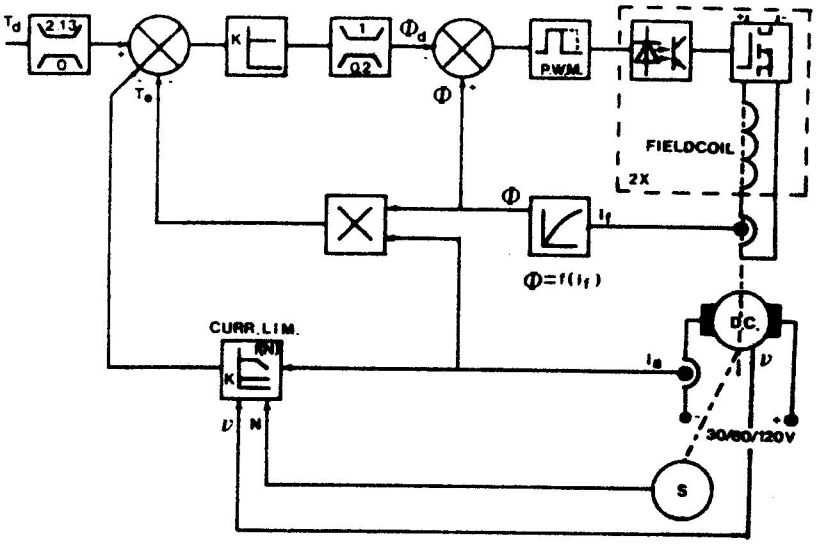

Fig. 10b. Torque control in the areas U=30, 60 and 120 V; R=60 mΩ

3.1. Field current controllers

The field current controllers are two-quadrant choppers implemented with power MOSFETs (see fig. 11a.). Due to the fact that the excitation voltage can be reversed, current changes can be accomplished with the same speed in both directions (see fig. 11b.).

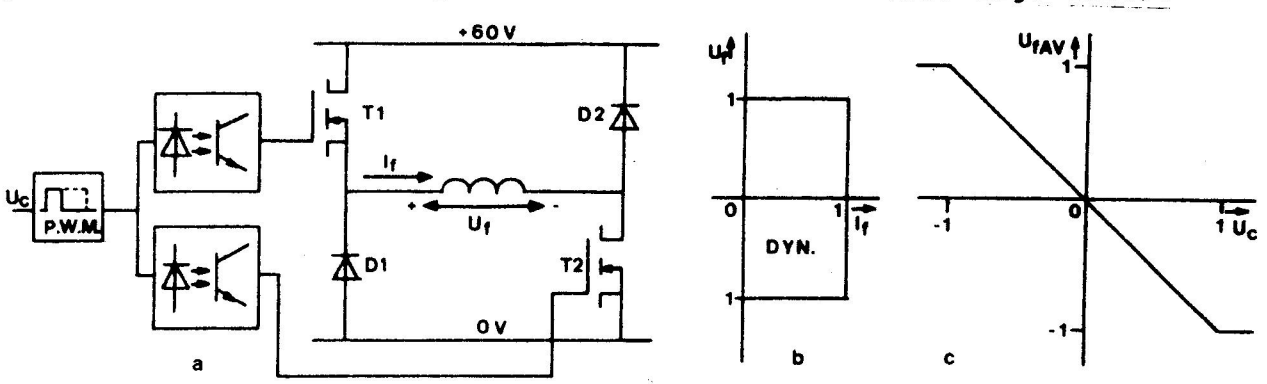

Fig. 11a. Field current chopper.
Fig. 11b. Two quadrant operation.
Fig. 11c. Excitation voltage vs. control voltage.

For a fast decrease of the field current, the energy stored in the field windings will be fed back into the battery via the diodes D1 and D2. The frequency of the PWM-signal is 400 Hz which is high enough to get a smooth current at a given field coil time constant of 100 ms. The average excitation voltage and, under stationary conditions, also the average current is proportional to the control voltage applied to the PW-modulator (fig. 11c.).

3.2. Measurement of the field

Due to the saturation of the magnetic circuit and hence non-linear relation between I_f and Φ_s, the field current cannot be used straightaway to determine the instantaneous EM-torque. Although, if the hysteresis is neglected, this function can be approximated quite accurately using the method of least squares, in practise it appeared to be satisfactory to make an even coarser approximation with three straight lines which remain all within the hysteresis curve (fig. 12).

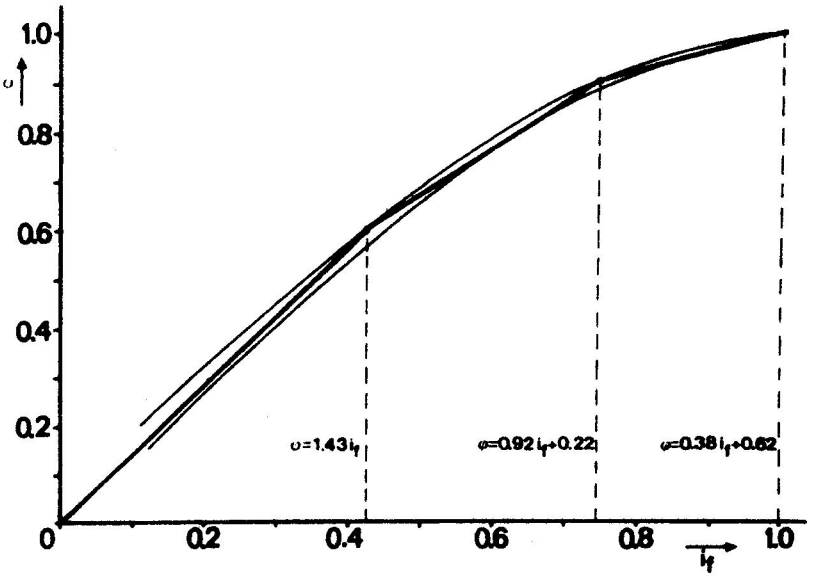

Fig. 12. Linear approximation of $\Phi_s = (I_f)$.

Based upon this approach the flux value is electronically obtained from the field current.

4. Flow chart and block diagram of voltage adjusting and field control

In order to change armature voltage under no-current conditions the current before opening the main switch and the voltage across the main switch before closing it in the new state, are forced to zero. Due to this program the field control operates successively under torque-, current-, and voltage control. The entire program is a complex structure which can best be understood by following the flow chart of fig. 14, together with the block diagram of fig. 15. Fig. 13 shows the voltage across the main

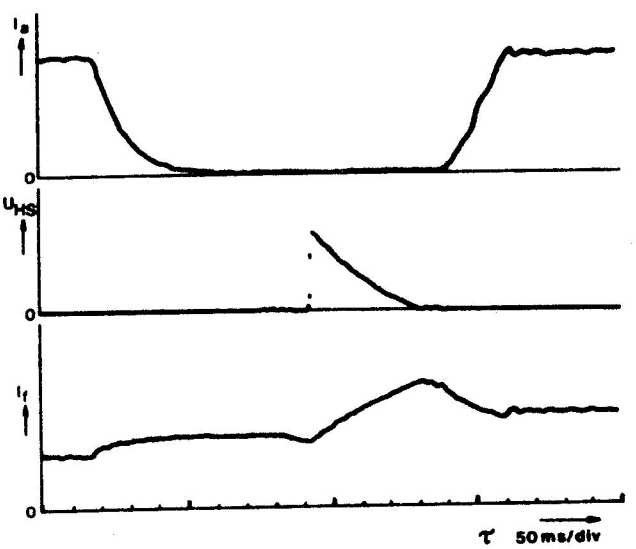

Fig. 13. Armature current, voltage across main switch and field current vs. time during switching to a higher voltage.

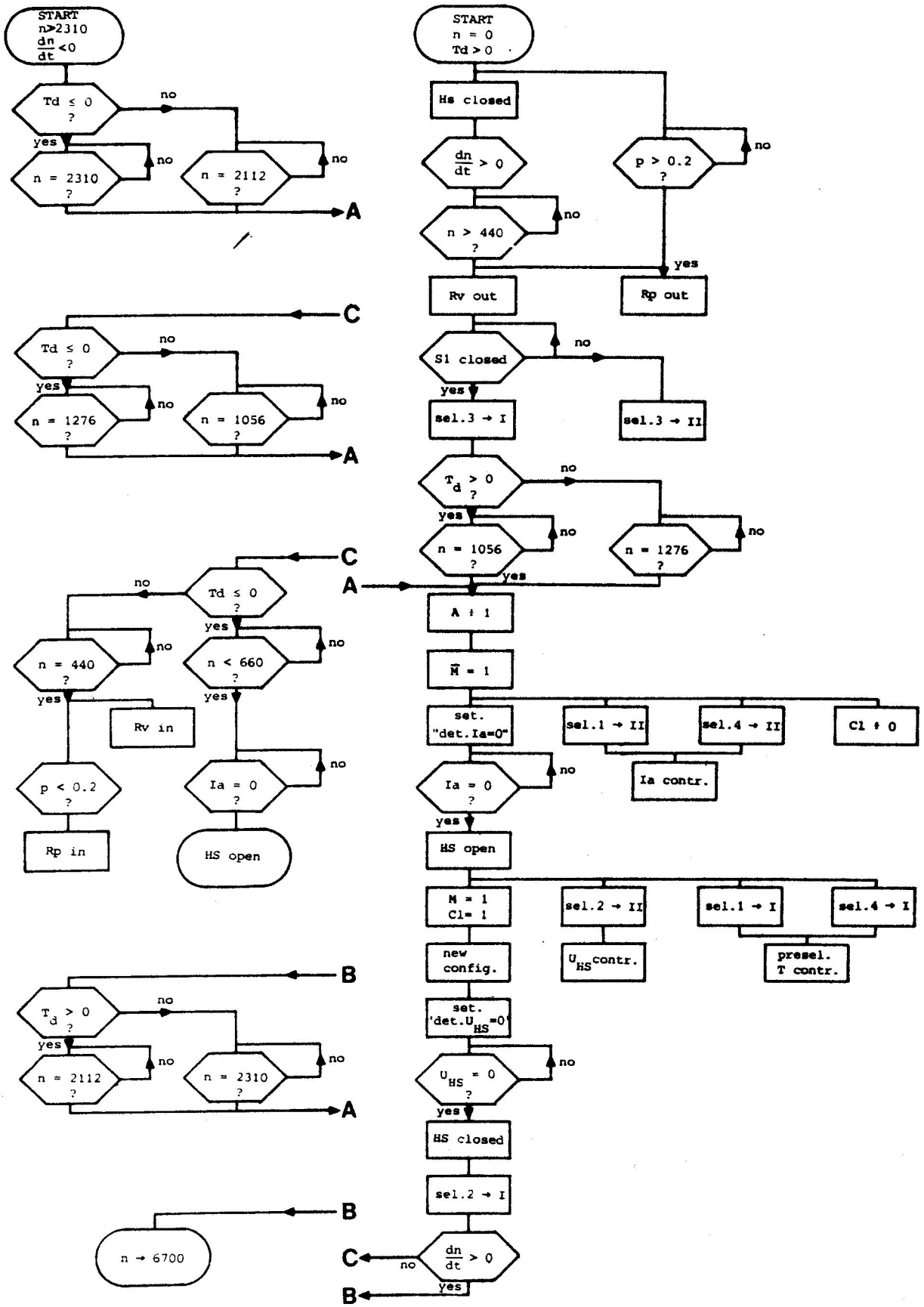

Fig. 14. Flow chart for accelerating and decellerating.

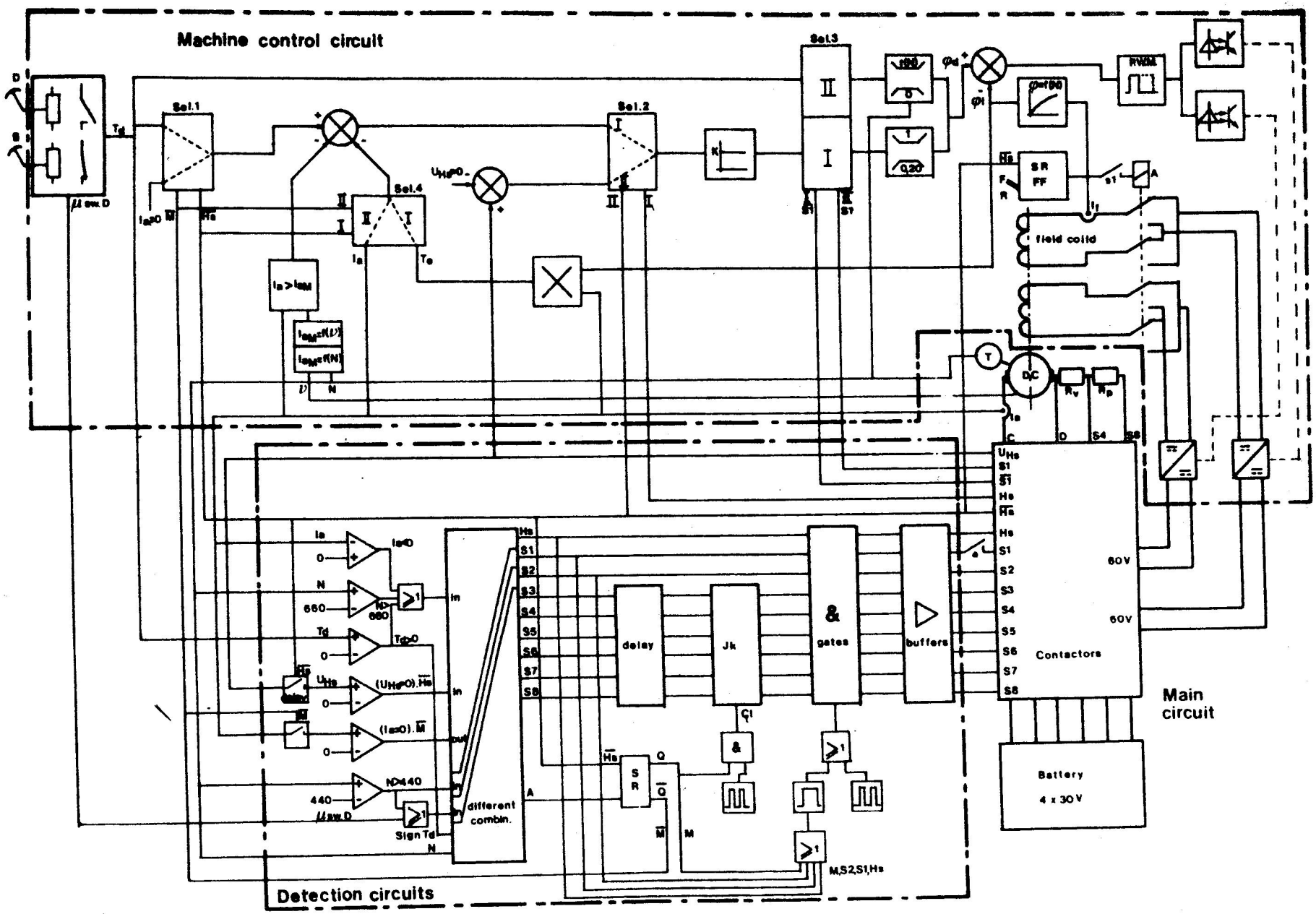

Fig. 15. Block diagram.

switch, the armature current and the field current during switching.

5. Conclusions

The conclusions drawn from the obtained test-bench results can be summarized as follows.

- It is possible to build a convenient speed control based upon a conventional circuit concept with use of modern control electronics.
- The control concept is probably very suitable to implement with microprocessor technology, which means that prices can be acceptable in larger series.
- The relatively low torque-armature current ratio, due to the field weakening, can be regarded as a disadvantage of this speed control.

6. Acknowledgements

The author wishes to express his thanks to professor J.A. Schot for reading the manuscript and to acknowledge his gratitude to Messrs. Barten, v.d. Boomen and Kremer, who are responsible for much of the realisation of this project.

List of symbols and subscripts

A_F	Front surface of car.
c_m	Machine constant.
c_w	Streamline constant.
E	Back E.M.F.
e	Normalized E.M.F.
F_t	Tractive effort.
f	Friction constant.
g	Gravity constant.
$H(s)$	Complex transfer function.
HS	Main switch.
I_a	Armature current.
I_f	Excitation current.
i_a	Normalized armature current.
i	Mechanical reduction.
J	Mechanical inertia.
L_a	Armature inductance.
L_f	Field coil inductance.
m	Mass of the vehicle.
N_s	Machine shaft speed.
p	Accelerator position.
R	Total armature circuit resistance.
R_a	Armature resistance.
R_f	Field coil resistance.
R_N	Nominal armature resistance $\frac{U_N}{I_{aN}}$.
R_p	Parking resistor.
R_v	Series resistor.
r	Normalized armature circuit resistance.
r_w	Wheel radius.
S	Switch
s	Laplace operator.
T_s	Machine shaft torque.
T_e	Electromagnetic torque.
T_{fr}	Friction torque
T_L	Load torque.
t_e	Normalized EM-torque.
U	Armature voltage.
U_b	Voltage drop across brushes.
U_f	Field coil voltage.
u	Normalized armature voltage.
V	Vehicle speed.
v	Normalized vehicle speed.

α	Slope angle.
λ	Constant.
ν	Field winding temperature.
ρ	Specific air density.
τ	Time.
Φ_a	Enclosed stator flux.
Φ_s	Stator flux.
φ	Normalized flux $\frac{\Phi_a}{\Phi_N}$
ω	Normalized angular speed.
Ω_s	Angular machine shaft speed.

Additional subscripts

AV	Average value.
L	Laplace domain.
M	Maximum.
m	Minimum.
N	Nominal.
O	Working point.
$\sim$	Small signals.

References

[1] Cool, J.C., Schijf, F.J., Viersma, T.J., Regeltechniek. Elsevier, Amsterdam/Brussel 1979.

[2] Dongen, L.A.M.van, "Aandrijflijnen voor elektrische voertuigen". Rapportnr. WV 155-043, T.H. Eindhoven 1979.

[3] Dongen, L.A.M.van, Graaf, R. van der, "The Eindhoven Experimental Vehicle: Vehicle Design and Drive Train", Drive Electric Amsterdam 1982.

[4] Dongen, L.A.M.van, Graaf, R. van der, Visscher, W.H.M., "Theoretical Prediction of Electric Vehicle Energy Consumption and Battery State-of Charge During Arbitrary Driving Cycles", EVC No. 8115, EVC Symposium VI Baltimore, Maryland.

[5] Dorf, R.C., Modern Control Systems, third edition. Addison-Wesley, Reading Massachusetts 1980.

[6] Jong, H.C.J. de, Kreek, J. van der, "De statische karakteristieken van de gelijkstroomcommutatormachine". Lecture notes EM 3615-0, group Electromechanics, T.H. Eindhoven.

[7] Koumans, W.A., "Electric car project of the Eindhoven University of Technology". PPL Conference Publication number 14, pp 87-90.

[8] Pfaff, G., Reglung Elektrischen Antriebe I: Eigenschaften, Gleichungen und Strukturbilder der Motoren. R. Oldenbourg Verlag, München und Wien 1971.

[9] Siemens A.G., Gleichstrom-Fahrmotor 1GV1: Technische Beschreibung.

[10] Visscher, W. Dongen, L.A.M.van, "Battery State-of Charge Model for Driving Cycle Operation". Drive Electric Amsterdam 1982.